Gravity Core Geochemistry at the Kronebreen Glacier, Svalbard, Norway: Quantifying Climate Flux in a Glacimarine Setting

Daren McGregor

Colby Geology

May 17, 2012

ABSTRACT

Six sediment gravity cores were collected along two east-west transects perpendicular to the ice front of Kronebreen, a tidewater glacier at the head of the northwest-trending Kongsfjorden, Svalbard, as part of an NSF-supported Research Experience for Undergraduates in the summer of 2011. Svalbard is an archipelago in the North Atlantic Ocean with a variety of terrains that makes it conducive to studying different aspects of the Holocene geologic record. Sediments throughout the archipelago capture Holocene and modern proxies for past climate fluctuation. Rapid sedimentation rates in Kongsfjorden during glacial retreat have resulted in a high-resolution record of the past few decades. This study looks at the sediment-core geochemistry and lithology of the sediments on the floor of Kongsfjorden in a chronostratigraphic framework, using a variety of analytical techniques. This study represents a multidisciplinary application of X-ray fluorescence, total organic content, Pb-210 radioisotopic dating, and other methods of sediment core analysis to infer paleoclimatic states. The sediments within the cores are composed primarily of reddish brown silty clay interbedded with black fine-sandy silt. These two types of sediment were classified into two facies, F1 and F3. Although there are several mechanisms for sediment deposition in the fjord environment, the dominant method is pelagic settling of sediment, evidenced by mm-scale lamination and a lack of turbidites in all sediment cores. As distance from the Kronebreen ice front increases, the amount of pelagic sediment in the sediment cores increases, indicating that ice-front processes are a trigger for turbidity events, and the influence of those processes decreases distally. This trend is supported by Ca/Fe ratios. Sea-ice fluctuation in recent years has undermined the reliability of “black layers” as a seasonal sedimentary event that can be used for estimating sediment ages and sedimentation rates, although Ca/Fe profiles indicate some form of periodicity that may be useful toward ascertaining ages. Pb-210 dating was unsuccessful, although quantitative counting of Ca-Fe periodicity can be used as a relative chronology.

INTRODUCTION

During the present period of climate flux, attempts are being made to understand and constrain the way in which Earth responds to these changes, as well as what these changes mean for life on the planet. The polar regions (the Arctic and Antarctic) are particularly sensitive to climatic perturbations, and they house extensive evidence of the impact that warming has had in the past, from changing ocean chemistries to the relationship between glacial retreat and fluctuations in sea level.

Since 2004, a National Science Foundation-funded summer Research Experience for Undergraduates has taken rising geoscience seniors or those in related fields to Svalbard, Norway. Svalbard is an archipelago in the North Atlantic Ocean (Fig. 1) with a variety of terrains that makes it conducive to studying different aspects of the Holocene geologic record. Sediments throughout the archipelago capture Holocene and modern proxies for past climate fluctuation. The summer's 2011 project was based in Kongsfjorden, a northwest-trending fjord with two actively retreating tidewater glaciers (Kronebreen and Kongsvegen) at its head (Fig. 2). Rapid sedimentation rates in Kongsfjorden during glacial retreat have resulted in a high-resolution record of the past few decades. Although students throughout the years have pursued various individual projects, the program has three specific overarching goals: (1) to explore the links in environmental processes between climate, glacial, fluvial lacustrine, and fjord systems; (2) to understand how measured environmental changes are expressed in the sediment record; and (3) to derive conclusions from the current sedimentation record and apply them to the historic record (Svalbard REU Program, 2004).

Global climate change effects are expected to be more extreme in the Arctic than at lower latitudes as a result of polar amplification, whereby ice and snow retreat reduces albedo in a positive feedback (Overpeck et al., 1997). Evidence of such an effect was observed in 2007 and

2008, with those years showing the lowest and second lowest ice extent ever recorded (NSIDC, 2009). Given the significant influence of Arctic change on global climate patterns associated with thermohaline circulation and atmospheric circulation, it is important that the effects of climate change on these systems are well understood (Overpeck et al., 1997). Accordingly, the status of such systems must be monitored today to generate baseline data upon which future comparison and predictions can be made (i.e., Blaszczyk et al., 2009).

There is a particular interest in the relative stability of Arctic tidewater glaciers in light of their susceptibility to a warmer environment that will induce higher calving rates, negative mass balance, and ultimately contribute to global eustatic sea-level rise (Powell, 1991; Blaszczyk et al., 2009). Given the difficult working conditions proximal to actively calving tidewater glaciers, there is a limited amount of data characterizing such systems. The Kronebreen-Kongsvegen glacier complex in Kongsfjorden, Svalbard, is amongst the most actively studied glacial systems in the Arctic as a result of its close proximity to the international research facilities located in Ny Ålesund (Svendsen et al., 2002, Blaszczyk et al., 2009).

During the 2011 field season, twenty-nine gravity cores were collected in front of the Kronebreen ice face as part of an REU project. Six of these cores were subjected to a variety of laboratory analyses to answer the following questions: Are there chemical patterns and relationships that change with respect to distance from the glacier/ seaward of the fjord? By assessing the geochemistry (and paleontology) of the mud on the fjord-floor, can we differentiate between the glacier-derived and the ocean-derived sediments? What is the dominant factor responsible for sedimentation? Can we calculate sedimentation rates and figure out whether or not these are changing over time? If the present glacial recession is triggered by global warming, how is this reflected in the fjord-floor sedimentology?

Svalbard

The Svalbard archipelago extends from 74°N - 81°N latitude and 10°E - 35°E longitude (Fig. 1). Kongsfjorden is a 22-km-long, 4- to 12-km-wide glacial fjord system situated on the west coast of Spitsbergen, the largest island in the archipelago. The catchment area of Kongsfjorden is 1260km^2, ~80% of which is glaciated by four tidewater glaciers along the northeastern coast and cirque glaciers along the southern coast]

Bedrock Geology

Kongsfjorden is divided by the Tertiary fold-thrust belt of western Spitsbergen to the southwest and the Proterozoic metamorphics to the northeast. The bedrock lithology underlying the Kronebreen and Kongsvegen glaciers include Proterozoic phyllite, carbonates, and schists; Devonian sandstone, conglomerate, and localized marble; and Carboniferous-Permian red sandstone, shale, and coal., The Kongsfjorden basin was likely carved out by Kongsvegen along a morphological depression induced by bedrock fracturing parallel to the thrust front (Svendsen et al., 2002; Dallmann, 1999).

The Quaternary geologic history of Svalbard is dominated by ice ages with intervening warming episodes. On at least one occasion during the Quaternary, an ice sheet covered the entire archipelago (Hjelle, 1993). During the last glacial cycle, the Wisconsinan (referred to as the Weischel in Europe), Svalbard was subject to two or three major glacial advances, where a major ice sheet grew in the Barents Sea and extended over, or confluenced with, an ice sheet over Svalbard. During their peak, glaciers extended in fjords and troughs out to the shelf break west of Spitsbergen. The last major glaciation on Svalbard, during the so called Late Weichselian (25,000-10,000 YBP), ended with a rapid deglaciation during the period ca. 14,000-10,000 BP. Transgression by the sea subsequent to deglaciation left marine terraces and flights of raised beaches around Svalbard. During the early Holocene, Svalbard glaciers were probably smaller

than at present, and the early Holocene climate was considerably milder. Most present cirque-and-valley glaciers were carved after 2500 BP. Glaciers expanded considerably during the so-called Little Ice Age, which culminated on Svalbard during the first decade of the 20th Century. Since then, most glaciers have retreated, likely as a consequence of the considerable warming occurring in the period after ca. 1915 (Hjelle, 1993; Ingolfsson, 2008).

Fjord-Water Circulation

Two regional water masses flow northward along the mouth of Kongsfjorden: 1) relatively cold and fresh Arctic Water traveling along the West Spitsbergen Shelf (WSS), and 2) relatively warm and saline Atlantic Water traveling within the West Spitsbergen Current (WSC) along the shelf slope (Poppick, 2010). An oceanic front that develops with the WSC along the WSS allows Arctic and Atlantic water masses to mix and exchange, forming Transformed Atlantic Water (TAW) (Svendsen et al., 2002). Due to the lack of a bedrock sill at the opening of Kongsfjorden, Atlantic water mixes with intermediate and deep fjord waters, particularly during summer months when frontal instabilities occur at the shelf break (Cottier et al., 2005; MacLachlan et al., 2007). The corresponding variation and gradient in heat and salinity drives local glacial retreat and advance, calving rate, freshwater flux, and sediment flux such that the fjord and surrounding glaciers fall within the subpolar rather than polar regime despite their polar latitude (Hop et al., 2002). Accordingly, the tidewater glaciers flowing into the fjord are polythermal, where the ice mass below the pressure melting point is temperate while the ice mass above this point reaches sub-freezing temperatures (Blaszczyk et al., 2009). The forces that drive fjord circulation in Kongsfjorden vary on a range of time scales, with prominent patterns being yearly variation in atmospheric climate conditions and heat transport in the WSC, seasonal variation in radiation from the sun, and daily variation of wind and tides (Svendsen et al., 2002).

The relative influence of temperature, salinity, and suspended sediment concentration on

water-column stratification changes within the fjord as a result of seasonal and bathymetric variability. During the summer meltwater season, freshwater input from submarine and glaciofluvial discharge at tidewater termini and atmospheric heating of surface waters induce more stable stratification (Svendsen et al., 2002). During this period, the pycnocline becomes impenetrable to winds, resulting in independent circulation of surface- and deep-water masses (Zaborska and Pempkowiak, 2006).

Kongsfjorden Climate and Climate Change

The parameters that govern Svalbard climate, and apply to the local climate in Kongsfjorden, include annual variation in light conditions, Arctic sea-ice extent, atmospheric general circulation, and ocean currents (Svendsen et al., 2002). In Kongsfjorden, the sun remains below the horizon from 25 October to 17 February, and remains above the horizon from 18 April to 23 August (Svendsen et al., 2002). The snow-free season generally lasts 94 days and induces local albedo decrease to ~10% from the snow season average of 80%. Highest precipitation occurs in March, September, and late November (Winther et al., 2002).

As an open fjord system exchanging water masses from lower latitudes, Kongsfjorden is particularly vulnerable to changes in WSC temperature and salinity induced by global climate change. Existing research shows that the amount and temperature of the Atlantic Water in the WSC has increased in recent years, and that the Arctic ice extent, within Kongsfjorden and beyond, has diminished (Blaszczyk et al., 2009; Kwok, 2009). Fast ice has historically developed in inner Kongsfjorden during December/January and reached a total thickness of 1 m, but has recently diminished in thickness and extent, leaving Kongsfjorden partially open during the winter (MacLachlan et al., 2007; Zajaczkowski et al., 2009). These effects are expected to increase in the coming decades (Svendsen et al., 2002).

The shifts in the WSC parallel an increasingly positive North Atlantic Oscillation Index

(NAO) over the past 30 years (Blaszczyk et al., 2009; Hurrell, 1995). The NAO index reflects the relative intensity of the sea-level pressure contrast between the Icelandic low- pressure center and the Azores high-pressure center. A high NAO, or positive index, produces stronger-than-average westerlies across the midlatitudes, bringing warmer and wetter conditions in Northern Europe and Scandinavia (Visbeck et al., 2001).

Kronebreen is a surging polythermal glacier that drains the Isachsen and Holtedahlfonna icefields. Its peak-flow velocity occurs during early July at 4.5 m/d (meters per day) when basal sliding is at its maximum and subsides to a winter average of 2 m/d, amounting to a maximum ice velocity of 785 m/a (meters per annum) (Bennett et al., 1999; Svendsen et al., 2002). The glacier's high velocity implies significant basal sliding and melting, and induces correlatively high calving rates. Thus, in this environment, calving is the main process of ablation and determines the net position of the terminus (Fischer and Powell, 1998). Calving is particularly prevalent within several hundred meters of the subglacial meltwater conduit (Trusel et al., 2009). Based on mapped submarine moraines, Kronebreen is inferred to have reached its maximum Holocene extent in 1869, ~11 km from the current terminus. During the second half of the 20th Century, the glacier front retreated ~150 m/a (Trusel et al., 2009).

Kongsvegen

Kongsvegen is a 27 km-long surge-type polythermal glacier that is fed primarily by two tributaries, Kongsvegen and Sidevegen. Having last surged in 1948, it is currently in its quiescent phase with a relatively slow velocity of 2.6 m/a (Melvold and Hagen, 1998). It flows in a northwesterly direction from 800 m above sea level to the ocean (at Kongsfjorden) with a surface slope between 0.5° and 2.5°. Its confluence with Kronebreen is approximately 5 km from the calving front and is marked by a medial moraine. Prior to 1990, the Kongsvegen terminus ended entirely in Kongsfjorden. The glacier front continues to actively calve along the northern

margin.

As with terrestrial glacial mass balance, tidewater glacial mass balance is a function of snow accumulation rate, ablation rate, and glacier flow velocity. While the parameters that drive snow accumulation are the same for terrestrial and tidewater glaciers, mechanisms of ablation and glacier-flow velocity are more complex at a tidewater terminus than at a terrestrial terminus. Tidewater-terminus ablation is predominantly a function of atmospheric melting and calving rates, with relatively minor influence from seawater melting (Powell, 1991). Calving rate is considered to be a function of, and positively correlated with, water depth at the terminus, degree of crevassing, and ice temperature (Powell, 1991). Calving is more frequent at stream discharges, forming embayments in the ice front (Powell, 1983). Glacier-flow velocity is mainly controlled by the presence of wind, rain, and daily tidal fluctuations, whereby rain, down-glacier wind, and high amplitude tidal ranges all increase ice-flow velocity (Fischer and Powell, 1998; O'Neel, 2000). Sedimentation rate is a secondary function of mass-balance, whereby high sedimentation can induce glacier advance due to stabilization of the grounding-line (Alley et al., 2007). Specifically, tall and steep sediment bodies deposited between ice and water reduce iceberg calving and stabilize the grounding line.

Glacimarine deposition

The main mechanisms of glacimarine-sediment deposition include suspension settling, sediment mass flow, and iceberg rafting (Cowan and Powell, 1991). The relative importance of each process across the ice face will depend on tidal mixing, the magnitude of meltwater discharge, the occurrence of slope failure from sediment oversteepening, and the transport of suspended sediment vertically and horizontally in the water column (Zajaczowski and Wlodarska-Lowalczuk, 2007). Frontal retreat rates also can control sediment depositional patterns by manipulating environmental energy at the ice front (Powell, 1983).

Deposition via suspension settling will dominate in regions proximal to a turbid meltwater plume. In such regions, meltwater initially travels as a horizontal jet and transports sediment along the fjord floor until internal turbulence decreases enough to allow the jet to buoyantly rise as a turbid overflow plume (Powell, 1990). Sediment in the overflow plume is released gradually from suspension as current velocity and/or meltwater discharge decreases.

As particles settle from suspension, coarser grains settle first, forming graded laminae that are subsequently overlain by massive laminae of flocculated finer material. These couplets are termed cyclopsams or cyclopels depending on grain size, whereby cyclopels are the finer-grained, distal counterparts of cyclopsams. Cyclopsams generally develop in regions down-fjord of the ice front where the current velocity is sufficient to transport large quantities of sand in suspension (Stewart, 1991). Cyclopels have been observed several kilometers from the ice face in temperate Alaskan fjords where sedimentation rates are high enough to limit in-faunal activity, but are less frequently preserved at such distances in subpolar West Spitsbergen fjords where lower sedimentation rates permit bioturbation (Cowan et al., 1998; Boulton, 1990).

Cyclopsams and cyclopels can occur in rhythmically laminated packages that have been attributed to semidiurnal tidal changes in Alaskan fjords (Cowan and Powell, 2007). During the slack low tide, horizontal current and vertical eddy velocities decrease enough to release a pulse of suspended sediment from the base of the overflow plume (Cowan and Powell, 1990). Two couplets are deposited each day, and are thickest during fortnightly spring/neap periods. Once identified as tidal rhythmites, these sequences can be useful in comparing changes in sedimentation rates over a given meltwater season (Cowan and Powell, 2007).

Rhythmically laminated sequences are not well preserved in proximal glaciomarine environments on account of the prevalence of sediment reworking in these regions. Often in the form of sediment mass flows, sediment reworking is common in proximal glaciomarine settings

as a result of high sediment accumulation rates that promote slope oversteepening, frequent calving events from above sea level that disturb sea floor sediment, and basal ice calving from the grounding line that disrupt sediment piled against the ice margin (Powell, 2005). Mass flows can occur fan-wide or locally within the fan, and can be driven by fluid density difference or gravity (Powell, 2005; Zajaczkowski and Wlodarska-Kowalczuk, 2007). A turbidity current, or hyperpycnal flow, is a type of sediment mass flow that results from the density gradient produced by dense, sediment-rich water flowing within sediment-poor ambient fluid (Powell, 2005). Turbidity currents can carry sediments many kilometers from a given ice margin, over a seafloor inclined as little as 0.03°, and produce deposits termed 'turbidites' (Zajaczkowski and Wlodarska-Kowalczuk, 2007).

Iceberg rafting occurs at spatially irregular intervals because icebergs melt and release sediment at various rates while traveling down-fjord. Sand and mud from a single discharge will disperse laterally if the current velocity exceeds the settling velocity, producing deposits indistinguishable from those that have settled from the overflow plume. Debris rafted via icebergs and sea ice (IRD-Ice Rafted Debris) is generally indistinguishable in the sediment record (Gilbert, 1990).

Sedimentation in front of Kronebreen/Kongsvegen

The above described mechanisms of deposition are expected to occur across the Kronebreen-Kongsvegen margin. The relative importance of each mechanism will vary spatially according to proximity to the two main depositional sources in front of the complex. These depocenters include a grounding-line fan in front of the Kronebreen submarine meltwater conduit, and an ice- contact delta in front of the Kongsvegen ice-marginal stream.

The majority of suspended sediment at the head of Kongsfjorden comes from the Kronebreen meltwater plume rather than the Kongsvegen ice-marginal stream, a reversal that

has occurred within the last 25 years (Trusel et al., 2009). In 2005, sedimentation rates of 30.5 cm/yr and 6.35 cm/yr were estimated from sediment traps proximal (240 m) and distal (470 m) to the Kronebreen meltwater plume, and rates of 6.94 cm/yr and 8.83 cm/yr were estimated for sites proximal (200 m) and distal (1,200 m) to the Kongsvegen ice-marginal stream (Trusel et al., 2009).

MATERIALS AND METHODS

FIELD METHODS-JULY 2011

From July 23, 2011, to July 27, 2011, twenty-nine sediment-gravity cores (Table 1) were collected along six geospatial transects within Kongsfjorden. The sediment cores were collected from within 1-6 km from the Kronebreen glacial margin. The cores were designated using a chronological nomenclature (i.e., the first core taken was GC-1, the last was GC-29), and each core has a unique set of GPS coordinates referring to the sampling location. For the scope of this research study, six cores were analyzed, and the rest were archived or used for projects undertaken by other researchers.

Core Collection

Sampling-location coordinates were decided using Google-Earth-image overlays of surface maps and aerial photos of Kongsfjorden. Each coordinate also was paired with an estimated fjord depth estimated using bathymetric maps developed during past REU projects. Within the study area, fjord-floor depths approached 100 m in some areas. In addition to following inferred sediment transport, the six collection sites form a semicircle around a basin-like structure on the fjord-floor (Fig. 3). One sediment core, GC-29, was somewhat isolated from this basin by a north-south trending ridge, which could affect sedimentation. After the collection-site coordinates were finalized, on each field day, coordinates were entered into the boat GPS as waypoints for sample collection.

The craft used for fieldwork was a 21-foot Polarcirkel 660® equipped with a gravity coring apparatus. The coring setup consisted of an aluminum winch wound with aircraft cable that was deployed off of the edge of boat. The winch also had a depth counter such that sampler-impact depths could be compared with estimated bathymetry.

A 20-kg Wildco® KB gravity-corer head with a 1 m-long core barrel loaded with a core liner, eggshell-core catcher, and aluminum-alloy nose was used to collect samples (Fig. 4). Based on estimated depth, the researcher powering the winch lowered the KB corer to within 10 m of the fjord floor. The winch was released, allowing the corer to free-fall until impacting the substrate. After impact and (hopeful) sediment penetration, the corer was reeled back to the surface, hoisted over the edge of the boat, and stood on the floor of the boat in vertical orientation. In a multi-step process (Fig. 5) involving three researchers, (1) the KB corer was lifted, (2) the core nose was removed and replaced with a orange core cap on the core bottom, (3) and the 20-kg core-barrel and head were lifted off of the core liner, all with the vertical orientation maintained to minimize perturbation of the sample. The top of the core liner was then covered with an orange cap labeled "top" as well as with the designated sample number. Both ends were then sealed with electrical tape to prevent water leakage that could perturb sediment structure, and stored vertically until returned to the Vaskerilab laboratory facility and field base at Ny-Alesund (Fig. 2).

In the Ny-Alesund laboratory, the cores were stored vertically at room temperature (22^0C) and the top caps were removed to allow moisture to evaporate. After excess water was gone, floral foam was lodged between the sediment and the core cap to secure the samples for transatlantic transportation. At this point, six cores were earmarked for further laboratory analyses. The six cores (GC-12, 24, 25, 26, 27, and 29) were selected based on the following criteria: (1) presence within the inferred pathway of sub-glacial plume-sediment transport, (2) extent of stratigraphic record, or length, and (3) spatial relationship to other cores. Four of the cores (24, 25, 26, 27) were collected at the substrate below the sediment plume emanating from the subglacial stream of Kronebreen (Figure 3), and thus would give the most insight into the upwelling-dictated sedimentology. The six cores selected all had lengths in excess of 60 cm

(among the longest collected during the 2011 field season), in order to preserve the oldest possible sediment record. In addition to following the sediment plume, the sampling transect was also designed out of a desire to look at down-fjord patterns in sedimentology, as past sampling sites in the REU were more ice-proximal. At the end of the field season, all twenty-nine cores were shipped from Ny-Alesund to the University of Massachusetts-Amherst for further analyses or archival.

LABORATORY ANALYSES-NOVEMBER 2011

Splitting of Cores

The cores arrived at University of Massachusetts-Amherst on September 21, 2011, and were placed in cold storage. On November 19, 2011, the six cores (GC-12, 24, 25, 26, 27, and 29) selected for the current research project were split lengthwise at the UMass-Amherst Quaternary Lab. The sediment core liners were split using a specialized Geotek apparatus consisting of two parallel rotary saws along a sliding tray. The still-intact core was moved to an adjacent table with the cut parallel to the tabletop. Fishing line was used to separate the core halves, but a combination of paint scrapers and deionized water was also employed for unconsolidated cores that did not readily split. Once opened, cores were smoothed parallel to bedding for visual analysis. For each core, one half was designated for sampling and the counterpart was designated as archival. Samples were taken from each core for CHN laboratory analyses at Colby College and Cs-137 and Pb-210 dating at University of Maine-Orono. The initial core descriptions and MSCL-S analyses were conducted over four days.

Initial Core Description

The sediment cores were initially logged and measured during which time lithologies, colors (categorized using Munsell color charts), and any other characters or horizons that were

of interest were described. The cores were air-dried for analysis on the Geotek MSCL-S scanner to a point where surface reflectivity was minimized.

MSCL-S Scanner

The GEOTEK MSCL-S consists of a modular tray apparatus with various sensors that perform parallel analyses on a sediment core, alongside high-resolution digital photography. All six cores were scanned for (1) gamma ray attenuation, (2) p-wave velocity, (3) magnetic susceptibility, and (4) color spectrophotometry. These metrics are useful not only for observing changes within a single core, but inter-core correlation.

Gamma Ray Attenuation

Gamma ray attenuation functions as an indicator of wet-bulk density in the core. A Cesium-137 gamma radiation source emits a narrow beam of gamma particles. Photons travel through the core and into a gamma-ray detector that is opposite the Cs-137 source. Incident photons are scattered by the electrons in the core with a partial energy loss, or attenuation. The attenuation, therefore, is directly related to the number of electrons in the sample (core thickness and electron density). By measuring the number of transmitted gamma photons that pass through the core unattenuated, the density of the core material can be determined.

Magnetic Susceptibility

Magnetic susceptibility is the extent and character of magnetization of a material in response to an applied magnetic field. If magnetic susceptibility is positive, then the magnetic field is strengthened by the presence of the material. Alternatively, if magnetic susceptibility is negative, the magnetic field is weakened in the presence of the material. The MSCL-S puts each core through a magnetic field generated by a loop sensor, and fluctuations in magnetic susceptibility in sediment cores are related to concentrations of magnetic or iron-bearing minerals and sedimentary provenance.

Color Spectrophotometry

The MSCL-S spectrophotometer allows for the observation of subtle shifts in color not discernible to the naked eye, within light wavelengths of 360 nm to 740 nm. A sensor captures light reflectivity off of the surface of the split core. Reflectivity can act as a reliable proxy for carbonate content. Color changes reflect shifts in lithology and sediment composition. In sediment cores of heterogeneous composition, changes in color spectrophotometry clearly mimic changes in lithology or chemical composition. In more homogenous cores, such as those in this study, the significant changes are less likely to be in color/chemical composition, and more likely to be observed in grain size. Nonetheless, spectrophotometry can be a useful tool for sediment core analyses.

LABORATORY ANALYSES-JANUARY 2012

ITRAX X-Ray Fluorescence and Radiography

From January 4, 2012, to January 19, 2012, the six cores were further analyzed using a Cox Analytical Systems ITRAX core scanner, which non-destructively irradiates the core in 5 mm intervals and simultaneously records both an XRF elemental profile and a radiograph of the sediment core. In interpreting the elemental profile, specific elemental concentrations and ratios can be correlated with environments of deposition. Depending on the type of emitter used for irradiating the sample, the ITRAX is more sensitive to different elements in the periodic table, based on molar mass. Elements lighter than silica are not easily resolved. For this study, the primary elements of interest are calcium and iron, two elements that are abundant in the samples and heavy enough to be detected by the ITRAX. Elemental concentrations also can be used to infer sediment provenance relating to the bedrock beneath the Kronebreen glacier. The actual ITRAX readout consists of a spreadsheet with each column representing a unique element

and each row representing elemental counts (in parts per million) at each stratigraphic depth within the core.

CHN Analysis

At Colby College, representative samples of each facies from each core were analyzed for organic content using the PerkinElmer 2400 Series CHNS/O Elemental Analyzer. The analyzer incinerates microgram-scale samples and measures the combusted CO_2 to calculate the amounts of total organic matter when compared against an acetanide standard. The samples are heated at temperatures in excess of 900^0 C and fully combusted with excess O_2. The elements that react in this process are carbon, hydrogen, and nitrogen. The products of this combustion reaction are carbon dioxide (CO_2), water (H_2O), and nitric oxide (NO). These product compounds are collected and weighed within the CHNS/O analyzer, and the weights are used to determine the elemental composition of the analyzed sample (by dividing mass of products by known molar weights) against the standard. Because there was a carbonate component in the cores, each sample was treated with 0.10 M hydrochloric acid to dissolve non-organic carbon, heated to evaporate excess reactant, and then subjected to CHN analysis.

Pb-210 Dating—UMaine-Orono

Sediment samples from GC-29 were sent to UMaine for Pb-210 dating. Although there are numerous types of radiometric dating of geologic materials, the likely age of the oldest sediments in the cores (<20 years) eliminated several potential techniques. The short half-life of Pb-210 (22.2 years) makes it ideally suited to the dating of historical age sediments (Dickin, 2005). Pb-210 occurs naturally as part of the uranium-238 decay chain. The relevant decay sequence is: $^{238}U \rightarrow ^{234}U \rightarrow ^{230}Th \rightarrow ^{226}Ra \rightarrow ^{222}Rn \rightarrow ^{218}Po \rightarrow ^{210}Pb \rightarrow ^{210}Po$. Pb-210 dating actually looks at the amount of excess polonium-210 to determine isotopic counts. If log [excess Po-210] is plotted as a function of accumulated dry weight of sediment, the line through the data should

be a straight line. Excess Po-210 is the amount of the Po-210 isotope that is in excess to the background Po-210 produced in the sediments by Ra-226. The excess Po-210 is thus assumed to be from direct atmospheric deposition of Pb-210 plus the import of Pb-210 from oceanic flow. It is also assumed in this analysis that the rates of isotope input and sediment input are roughly constant over time. The accuracy of Pb-210 dating depends on the whether or not the isotopic counts are high enough to enable detection, as well as the absence of any external pollution that could contaminate the Pb-210 signature of the sediment. In the analysis of GC-29, counts of Pb-210 within the core were found to be at levels that were too low for effective construction of an accurate age throughout the sediment core.

RESULTS

Qualitative and quantitative analytical results for each sediment core are described below, in numerical order. In general, two facies were encountered: (F1) a dominant reddish brown silty clay and (F3) an odorous (sulfurous) black sandy silt that occurred in laminae of varying mm-scale thicknesses. Initial core description identified a second (F2) facies as well, but upon further investigation, that lithology was reclassified as F3. The radiographs of the cores also are discussed, if the x-rays illuminated lamination patterns that were not observable by eye. Lastly, Ca/Fe ratio maxima and minima are reported for each core, as well as TOC averages for cores GC-12, 25, 26, and 27. For all samples, the mean TOC of F1 sediments was 1.63%, and the mean TOC value of F3 sediments was 3.17%.

GC-12

General Stratigraphy

Sediment core GC-12 (Fig. 6, 7) is 60 cm long and collected 3.9 km from the ice margin at a fjord-floor depth of 98 m. Both sediment facies are observed. The first (F1) is the most common and composed of a reddish brown (Munsell 2.5 YR 4/3) silty clay. The second facies (F3), is a black (Munsell GLEY 2.5/N) fine-sandy silt that occurs in regular laminae interbedded with F1 at 1 cm intervals. F3 laminae are <0.5 mm in thickness and have a slight sulfurous odor consistent with that of organic material subjected to bacterial decay. The bottom contacts of the laminae are sharp and the top contacts grade into the overlying F1 facies.

The sediment column begins at a depth of -53 cm within the core. There are no characteristic structures to the facies beyond laminae. Beginning at 53 cm and continuing upsection to 19 cm there is a distinctive repeating sequence of two sediment packages: (1) a 1 cm-thick horizon of < 0.5 mm-thick F1 laminae that is overlain by (2) a 0.5 cm-thick horizon of < 0.5 mm-thick F3 laminae interbedded with F1 laminae. The grains within the F3 laminae are

coarser than the F1 laminae. These packages remain constant in thickness and periodicity throughout the sequence. There is a 2 mm-thick horizon of F3 laminae at 19 cm that contacts sharply with the underlying F1 interval. Greater variation is seen in the remainder of the core. From 18.5 cm to 17 cm, there are 0.5 mm-thick F1 laminae. From 17 cm to 14 cm, there is an interval of < 0.5 mm-thick F3 laminae interbedded with F1 laminae that are < 0.5 mm-thick. These display a coarser grain size than those in the underlying strata. F1 laminae, < 0.5 mm in thickness, dominate the interval from 14 cm to the top of the core; no F3 laminae occur in this section.

Geochemical Trends

The Ca/Fe ratio within GC-12 ranged from a low of 0.106 at a depth of 46.4 cm to a peak of 0.294 at a depth of 41.5 cm. The mean Ca/Fe ratio within the core was 0.226, with a standard deviation of 0.018.

Based on three measurements from each facies, the mean TOC value of F1 was 1.14%, and the mean TOC value of F3 was 2.13% (Table 2).

GC-24

General Stratigraphy

Sediment core GC-24 (Fig. 8, 9) is 71 cm long and collected 2.3 km from the ice margin at a fjord-floor depth of 60 m. The dominant F1 is a reddish brown (Munsell 2.5 YR 4/3) silty clay. The second facies (F3) is a black (Munsell GLEY 2.5/N) fine-sandy silt that occurs in laminae. The F3 laminae are generally < 0.5 cm in thickness and have a slight odor consistent with that of organic material that has decayed. The bottom contacts of all F3 laminae are sharp, with a gradational upper contact into the F1 facies.

The sediment column begins at a depth of -66.5 cm where there are < 0.5 mm-thickness F1 laminae interbedded with < 0.5 mm-thickness F3 laminae to 63 cm, with the F1 being the

dominant facies. At 63 cm, there is a 3 mm-thick horizon of < 0.5 mm-thickness F1 laminae interbedded with < 0.5 mm-thickness F3 laminae, but here the F3 dominates. From 62.5 cm to 58 cm, there are extremely fine F1 laminations on a scale of <0.5 mm. At 58 cm is a lens-shaped, convex-up bed that is 5 mm thick composed predominantly of < 0.5 mm-thick F3 laminae. The strata above and below this horizon do not display any curvature. From 57 cm to 31 cm, there is an interval of < 0.5 mm-thickness F1 laminae, with faint < 0.5 mm-thick F3 laminae interbedded every 1-3 cm. From 31 cm to 24 cm, there is an interval of significant 0.5 mm-thick F3 laminae. From 25 cm to 24 cm, the F3 laminae have a larger sand component. From 24 cm to 17 cm, there is a sequence of interbedded F1 and F3 laminae, with the grain size coarsening upward. At 17 cm, there is a coarse, 6 mm-thick horizon of F3 lithology, with no visible lamination. At 15 cm and 14 cm there are 3 mm-thick horizons of F3 laminae. From 14 cm to the top of the core, there are < 0.5 mm-thick F1 laminae with no visible F3 interbeds.

Geochemical Trends

The Ca/Fe ratio within GC-24 ranged from a low of 0.150 at a depth of 18.4 cm to a high of 0.291 at a depth of 10.9 cm. The mean Ca/Fe ratio within the core was 0.215, with a standard deviation of 0.017.

GC-25

General Stratigraphy

Sediment core GC-25 (Fig. 10, 11) is 64 cm long and collected 3.1 km from the ice margin at a fjord-floor depth of 62 m. The dominant (F1) facies is a reddish brown (Munsell 2.5 YR 4/3) silty clay, whereas the F3 facies is a black (Munsell GLEY 2.5/N) fine-sandy silt that occurs in only one thin lamina at a depth of 55 cm in the core. The F3 laminae is mm-scale in thickness. There is a dark gray dropstone at a depth of 39 cm. The bottom contact of the F3 lamina is sharp, and the top contact grades into type F1.

The sediment column of GC-25 begins at a depth of 64 cm within the core. The entire core is very homogenous and there is a marked absence of any sedimentary structures beyond laminae. Laminae of the F1 facies occur from 64 cm to 55 cm and alternate between < 0.5 mm to 1 mm-thickness throughout this interval. At 55 cm, there is a 4 mm-thick F3 interbed that has a greater silt component than the underlying strata. Directly above this horizon there is an abrupt return to the F1 facies that continues from 55 cm to 30 cm, where an interval of alternating <0.5 mm and 1 mm-thickness F1 laminae occurs. At 39 cm, there is a dropstone imprint. The interval from 30 cm to 28.5 cm contains < 0.5 mm-thick F1 laminae with more silt than clay. From 28.5 cm to the core top, there are 0.5 mm-thick F1 laminae.

Geochemical Trends

The Ca/Fe ratio within GC-25 ranged from a low of 0 (likely due to detection issues with ITRAX) at a depth of 58 cm to a peak of 0.339 at a depth of 17.3 cm. The mean Ca/Fe ratio within the core was 0.219, with a standard deviation of 0.043.

Based on three measurements from each facies, the mean TOC value of F1 was 2.06%, and the mean TOC value of F3 was 3.90% (Table 2).

GC-26

General Stratigraphy

Sediment core GC-26 (Fig. 12, 13) is 68 cm long and collected 4.1 km from the ice margin at a fjord-floor depth of 67 m. The dominant (F1) facies is a reddish brown (Munsell 2.5 YR 4/3) silty clay, whereas the F3 facies is a black (Munsell GLEY 2.5/N) fine-sandy silt that frequently occurs in irregular laminae, with intervals between F3 laminae ranging from 1-9 cm. The F3 laminae range from mm-scale to 2 cm in thickness. The bottom contacts of all F3 laminae are sharp, and the upper contacts grade into the F1 sediments.

The sediment column of GC-26 begins at a depth of 68 cm from the sediment-water interface where there are faint < 0.5 mm-thick F1 laminae, with no additional structure to the facies, continuing on to a depth of 61 cm. At this depth, there is a lens-shaped concave-up lamina consistent with the F1 facies that 1 mm in thickness. From 61 cm to 57 cm, there is a repetition of a package of a 1 cm-thick sequence of < 0.5 mm F1 laminae overlain by 1 mm-thick F1 lamina, with some interbedded F3 laminae. There is a faint alternation between < 0.5 mm F1 laminae and < 0.5 mm F3 laminae from 57 cm to 51.5 cm, with neither lithology dominating the interval. From 51.5 cm to 50.5 cm, there is an F3-dominated interval of F1 and F3 < 0.5 mm-thickness laminae. From 50.5 cm to 43.5 cm, there is an extended interval of only F1 fine-scale laminae. Over the next centimeter, there is an F3 dominated interval. From 42.5 cm to 31 cm, there is a package of 0.5 mm-thick F1 laminae with low (difficult to resolve) numbers of interbedded F3 laminae. The overlying interval, 31-29 cm, is predominantly F3 laminae. There are exclusively < 0.5 mm-thick F1 laminae from 29 cm to 14 cm. At 14 cm, there is a 7 mm-thick horizon of F3 laminae, mostly concentrated in the center of the core. From 14.5 cm to 8 cm, there is an interval of massive F1 mud (without visible laminae). At 8 cm and 6 cm, there are 5 mm-thick beds of F3 sediments, without laminae. From 5 cm until to the top of the sediment, there are < 0.5 mm-thickness F1 laminae.

Geochemical Trends

The Ca/Fe ratio within GC-26 ranged from a low of 0.152 at a depth of 60.6 cm to a peak of 0.286 at a depth of 20.4 cm. The mean Ca/Fe ratio within the core was 0.208, with a standard deviation of 0.022.

Based on three measurements from each facies, the mean TOC value of F1 was 1.38%, and the mean TOC value of F3 was 2.81% (Table 2).

GC-27

General Stratigraphy

Sediment core GC-27 (Fig. 14, 15) is 68 cm long and collected 5.4 km from the ice margin at a fjord-floor depth of 55 m. The dominant (F1) is a reddish brown (Munsell 2.5 YR 4/3) silty clay. The F3 facies is a black (Munsell GLEY 2.5/N) fine-sandy silt that occurs in irregular laminae in the top half of the core beginning at 35 cm depth. The F3 laminae are generally less than 1-2 cm in thickness with sharp bottom contacts of all F3 laminae, upper contacts grade into the F1.

The sediment column of GC-27 begins at a depth of 62 cm below the fjord-floor, where there are < 0.5 mm-thick laminae of the F1 facies up to 50 cm. Visible structures, other than laminae, are not obvious, and through this interval there are no overt changes in color or facies. At 50 cm, there is a convex- up 4 mm-thick lens of sandy sediment with the same color as the F1 facies. From 48 cm to 37 cm, there is another interval of < 0.5 mm-thick F1 without any additional structures, but frequently interbedded F3 laminae occur. These F3 laminae are of comparable thickness (~0.5 mm) to the F1 facies. From 37 cm to 32 cm, there is a similar interbedded pattern of F3 and F1 laminae, but with thicker F3 laminae. From 32 cm to 25 cm, there is a coarsening up sequence of 0.3 mm-thick F1 laminae, with an increasing sand fraction in the upper part of the interval. At 23.5 cm and 21.5 cm there are two lens-shaped, concave-up, 2 mm-thick F3 laminae. The concave shape may be an artifact of coring. From 21.5 cm to 16 cm, an interval of < 0.5 mm-thick F1 laminae with no visible additional structures is found. At 16 cm, there is a 4 mm-thick horizon of F3 laminae that grades upwards into the F1 facies. From 16 cm to the top of the core, there is an apparently massive (no visible lamina) F1 interval, although the core-splitting process may have obscured all primary sedimentary structures.

Geochemical Trends

The Ca/Fe ratio within GC-27 ranged from a minimum of 0.083 at a depth of 55.9 cm to a peak of 0.439 at a depth of 19.6 cm. The mean Ca/Fe ratio within the core was 0.246, with a standard deviation of 0.035.

Based on three measurements from each facies, the mean TOC value of F1 was 1.94%, and the mean TOC value of F3 was 3.85% (Table 2).

GC-29

General Stratigraphy

Sediment core GC-29 (Fig. 16, 17) is 61.5 cm long and collected 5.7 km from the ice margin at a fjord-floor depth of 49 m. The dominant facies (F1) is a reddish brown (Munsell 2.5 YR 4/3) silty clay that alternates with (F3) a black (Munsell GLEY 2.5/N) fine-sandy silt that occurs in regular, clearly-defined laminae every 2-5 cm within the core. The F3 laminae consistently range from 0.5-1 cm in thickness and have a slight odor consistent with that of organic material that has been subjected to bacterial decay. Thinner, harder-to-resolve F3 laminae also interbed on a fine scale. The bottom contacts of all F3 laminae are sharp, and the top contacts grade into the F1 sediments.

GC-29 begins at a depth of 56 cm in the core, with the densest material occurring from 56 cm to 41 cm (Fig. 11B). This configuration may be a function of compression from the weight of overlying sediment. Over the interval from 56-54 cm, F1 laminations are extremely fine, on a scale of <0.5 mm, with no additional visible sedimentary structures. There is a series of four laminations that are 1 mm in thickness, with 0.5 mm of massive sediments separating each lamina at 54 cm. These F1 lamina are interbedded with black F3 laminae. The F1 laminae cease at a depth of 53.5 cm, where F3 laminae extend up to a depth of 51.5 cm. Along this interval, the F3 laminae do not extend across the entire diameter of the core. From 51.5-50.5 cm, there is an interval of ~0.5 mm-scale laminated F1 facies in which there is an imprint of a dropstone

(removed during core splitting). At 50 cm, there is a 4 mm-thick horizon of the F3 facies, extending across the entire width of the core. From 50 cm to 47 cm, there are two repeating packages of an ~11 mm-thick series of fine F1 laminae overlain by a ~5 mm-thick horizon of F3, with the top contact of the F3 horizon graded, and the bottom contacts sharp. Beginning at a depth of 47 cm, there is an interval of < 0.5 mm-thick F1 laminae that continues for 9.5 cm. The grain size coarsens from clay to silt over this interval. There are two thick (5 mm) deposits of the F3 facies from 37.5-36 cm that do not extend across the entire width of the core, but, rather, the center 1.5 cm. There is a greater sand component to these sediments relative to other F3 laminae in the core. The radiograph shows a decrease in density from 41 cm to 36 cm, where there is a sharp grain size change to clay. Laminae of interbedding F1 and F3 facies occur from 36 cm to 34 cm, with the darker F3 forming a diagonal shape across the core. This interval also shows a corresponding increase in density based on the radiograph. From the interval of 34-27 cm, there are two sequences of 3 cm of fine-scale F1 laminae overlain by 5 mm-thick F3 laminae. From 27 cm to the top of the core, interbedded F1 and F3 laminae occur with thicknesses < 0.5 mm. No additional visible structures are seen in this facies.

Geochemical Trends

The Ca/Fe ratio within GC-29 ranged from a low of 0.164 at a depth of 30.4 cm to a peak of 0.564 at a depth of 47.8 cm. The mean Ca/Fe ratio within the core was 0.230, with a standard deviation of 0.020.

DISCUSSION

Facies F1

Multiple depositional processes can produce the mm-scale interlaminations that dominate the sediment cores. O' Cofaigh and Dowdeswell (2001) established that turbidity currents, suspension settling, and iceberg rafting (IRD) can create mm-scale laminations with sharp or gradational lower and upper contacts. Turbidity deposits have a distinctive sequence (Bouma, 1962) from bottom to top, of a thick massively fining-upward bed at the bottom, followed by a horizon of wavy sand ripple laminae, then a thin horizon of parallel laminae, and lastly a layer of clay-sized grains, but many of the components of this sequence, such as the diversity of grain size, are not present in any of the sediment cores, or cannot be effectively observed considering their height (~60 cm) and diameter (7.5 cm). Also, although turbidity currents can produce thin laminae, in general those that are < 10 mm in thickness are interpreted to have settled from suspension (Cowan et al., 1998). Suspension settling can be effectively defined as the passive deposition of sediment out of suspension in the water column. This type of deposition produces thin laminae, and finer material can settle coincidentally with coarser grains (O Cofaigh and Dowdeswell). IRD can occur in cores as lenses of coarse material or as dropstones within sediment. As icebergs calve from the face of the glacier and drift down-fjord, they accumulate sediment, and this sediment is deposited as the iceberg melts, forming a diamicton. In sediment cores, IRD can dominate the winter sediment supply, because there is relatively minimal meltwater discharge (Cowan and Powell, 2007). It is likely that suspension settling is the dominant depositional process for the laminated intervals of the sediment cores, and that turbidity currents may account for the massive portions of GC-26 and GC-27.

The Color of Facies F3

Similarly to past interpretations of sediments from Kongsfjorden (Poppick, 2009), the black (Munsell GLEY 2.5/N) fine-sandy silt of the F3 facies is interpreted to sediment stained by diagenetic iron monosulfide. Anaerobic sulfate-reducing bacteria produce sulfide that reacts with dissolved Fe^{2+} to form insoluble Fe monosulfides during the natural decomposition of organic matter (Smith and Melville, 2004). Past work (Hop et al., 2002) has asserted that this process may account for 60-90% or remineralization in some Svalbard fjords. Further, this is supported by the higher TOC ratios of F3 relative to F1 (Table 2).

Black/organic layers in sediment cores can be an effective tool for constraining annual sedimentation rates. If there is a consistent seasonal signal (i.e. spring phytoplankton blooms), then a rough estimate for sedimentation rates can be developed. However, Zajaczkowski and others (2009) have indicated that such processes may not be the norm in Kongsfjorden. In past years, the occurrence of spring phytoplankton blooms has varied significantly due to reduced winter sea ice cover. During periods of reduced sea ice cover, there is more predation of phytoplankton by zooplankton, resulting in a lesser amount of organic material settling on the fjord substrate and thus hindering the development of a characteristic seasonal black layer (Zajaczkowski et al., 2009). This fact undermines the reliability of F3 as an annual marker, although it does not totally negate it.

Ca/Fe ratio

Ca/Fe ratio reflects carbonate content and generally shows a strong correlation to sedimentary units. In general, turbidite sands, silts and muds, presumably sourced from shallower water, are richer in Fe and poorer in Ca than pelagic interbeds. The Ca/Fe profile shape within turbidites appears to mirror grading, or its absence, and provide clear indication of the textural subdivisions without the need for grain-size analysis. Bioturbative mixing of pelagite into the upper parts of turbidites causes the Ca/Fe ratio to decrease in the tops of the turbidite

units. Identification of textural subdivisions is important in assessing source distality–proximality relationships. Calcium peaks, or lack of Ca peaks (commonly associated with increased Si), within turbidite bases distinguish foraminifer- or shell-rich and more terrigenous quartz-rich bases (Rothwell et al., 2006). Based on initial analysis of Ca/Fe ratios, there is a clear variation in the energy of deposition (turbidite vs. settling) for the sediments for all of the cores. Negative excursions would represent turbidite sediments, as greater amounts of iron would lower the Ca/Fe ratio. Positive excursions, if interpreted solely as increases in terrigenous input, could also (in theory) be correlated to spring meltwater pulses. The Ca/Fe profiles of all six cores indicate much more positive excursions than negative excursions, reinforcing the implication from the structure of the F1 facies that most sediments were deposited pelagically. Further, as distance from the ice face for each core increases, there is also an increase in the Ca/Fe mean and maximum. As distance from the glacier increases, the fraction of pelagic deposition increases.

Dating, Chronology

This study would have benefited greatly from successful dating of sediments, to provide a chronostratigraphic framework. But the lack of success in our efforts for Pb-210 dating underscore the difficulty of acquiring ages for Kongsfjorden sediments. However, given that the half-life of Pb-210 is 22.3 years, this method is only applicable to cores that span multiple decades of sedimentation. Other studies (Zaborska et al., 2006) have performed Pb-210 analyses on Kongsfjorden sediments, so the failure of our attempt may just be a matter of bad luck.

In looking at periodicities of both Ca/Fe and ImageJ color excursions (Fig. 6-17), there is a somewhat apparent quantitative trend. GC-12, the most ice-proximal core, has the most well-defined Ca/Fe signal, and an arbitrary counting of distinctive peak/excursion indicates roughly 10-13 cycles. Given the work of other studies and known information about sedimentation rates

(Poppick, 2010), 10-13 years would be an unrealistic age for these cores, so the cycles are greater than annual. GC-29, the most ice-distal core and likely the oldest, captures 8-9 distinctively shaped repeating intervals within the Ca-Fe profile, although these excursions are much less defined. Poppick (2009) dated a stratigraphic horizon 30 cm below the substrate to the year 1986, correlating a spike in Cs-137 to the Chernobyl nuclear disaster. There is also the consideration of variable sedimentation rates through the years. Based on the extent of the glacier, some coring sites may have been under ice at certain points, so no core sampled represents an interval of even sedimentation. The defined intervals observed in the Ca/Fe ratios (10-13; 8-9) could indicate some form of multi-annual pattern akin to a NAO-type oscillation. If an age of 23 years (2009-1986) can be found 30 cm below the substrate, then it likely that the sediment cores used in this study, with lengths in excess of 60 cm, would definitely exceed that age, and perhaps preserve a sediment record in excess of 40-50 years, depending on sedimentation rates.

CONCLUSIONS

Kongsfjorden sediments collected along two east-west transects perpendicular to the Kronebreen ice front are composed primarily of reddish brown silty clay interbedded with black fine-sandy silt. These two types of sediment were classified into two facies, F1 and F3.

Although there are several mechanisms for sediment deposition in the fjord environment, the dominant method is pelagic settling of sediment, evidenced by mm-scale lamination and a lack of turbidites in all sediment cores. As distance from the Kronebreen ice front increases, the amount of pelagic sediment in the sediment cores increases, indicating that ice-front processes are a trigger for turbidity events, and the influence of those processes decreases distally. This trend is supported by Ca/Fe ratios.

Sea-ice fluctuation in recent years has undermined the reliability of “black layers” as a seasonal sedimentary event that can be used for estimating sediment ages and sedimentation rates, although Ca/Fe profiles indicate some form of periodicity that may be useful toward ascertaining ages. Pb-210 dating was unsuccessful.

This study represents an archive of the depositional environments and processes occurring within Kongsfjorden in a setting more distal to the glacier-face than previous studies, contributing to the study of this glacimarine system.

TABLES

Core Name	Date of Collection	Depth (m)	Latitude	Longitude
GC-12	7/24/11	98	78°54.021'	12°20.084'
GC-24	7/27/11	60	78°53.960'	12°29.693'
GC-25	7/27/11	62	78°54.228'	12°28.101'
GC-26	7/27/11	67	78°54.665'	12°26.304'
GC-27	7/27/11	55	78°55.079'	12°23.103'
GC-29	7/27/11	49	78°54.320'	12°18.950'

Table 1. Core numbers, dates of collection, depths below water surface, and coordinates.

Core Number and Facies	Depth within core	Calculated TOC value (F1)	Calculated TOC value (F3)

GC-12-F1-A	7 cm	0.98%	
GC-12-F1-B	10 cm	1.33%	
GC 12-F1-C	17 cm	1.10%	
GC-12-F3-A	43 cm		2.07%
GC-12-F3-B	46 cm		2.79%
GC-12-F3-C	47 cm		1.52%
	Locality Mean:	**1.14%**	**2.13%**
GC-25-F1-A	7 cm	1.47%	
GC-25-F1-B	14 cm	2.80%	
GC-25-F1-C	21 cm	1.91%	
GC-25-F3-A	52 cm		3.51%
GC-25-F3-B	54.5 cm		4.06%
GC-25-F3-C	56.5 cm		4.12%
	Locality Mean:	**2.06%**	**3.90%**
GC-26-F1-A	15 cm	1.72%	
GC-26-F1-B	16 cm	1.54%	
GC-26-F1-C	11 cm	0.87%	
GC-26-F3-A	24 cm		2.87%
GC-26-F3-B	25 cm		3.24%
GC-26-F3-C	26 cm		2.31%
	Locality Mean:	**1.38%**	**2.81%**
GC-27-F1-A	11 cm	1.90%	
GC-27-F1-B	13.5 cm	1.79%	
GC-27-F1-C	15 cm	2.14%	
GC-27-F3-A	21 cm		3.79%
GC-27-F3-B	22 cm		4.12%
GC-27-F3-C	24 cm		3.64%
	Locality Mean:	**1.94%**	**3.85%**
	Overall Mean F1	**1.63%**	
	Overall Mean F3		**3.17%**

Table 2. TOC values for F1 and F3 facies based on samples from GC-12, 25, 26, and 27.

FIGURES

Figure 1. Map of Svalbard, Norway. Kongsfjorden is on the western island of Spitsbergen. Taken from samadhisoft.com.

Figure 2. Map of Kongsfjorden, west Spitsbergen, Svalbard, Norway. Taken from the Norwegian Polar Institute.

Figure 3. Core collection sites. The cores studied in this project are GC-12, 24, 25, 26, 27, and 29, to the northwest of the photo. Image created with Google Earth.

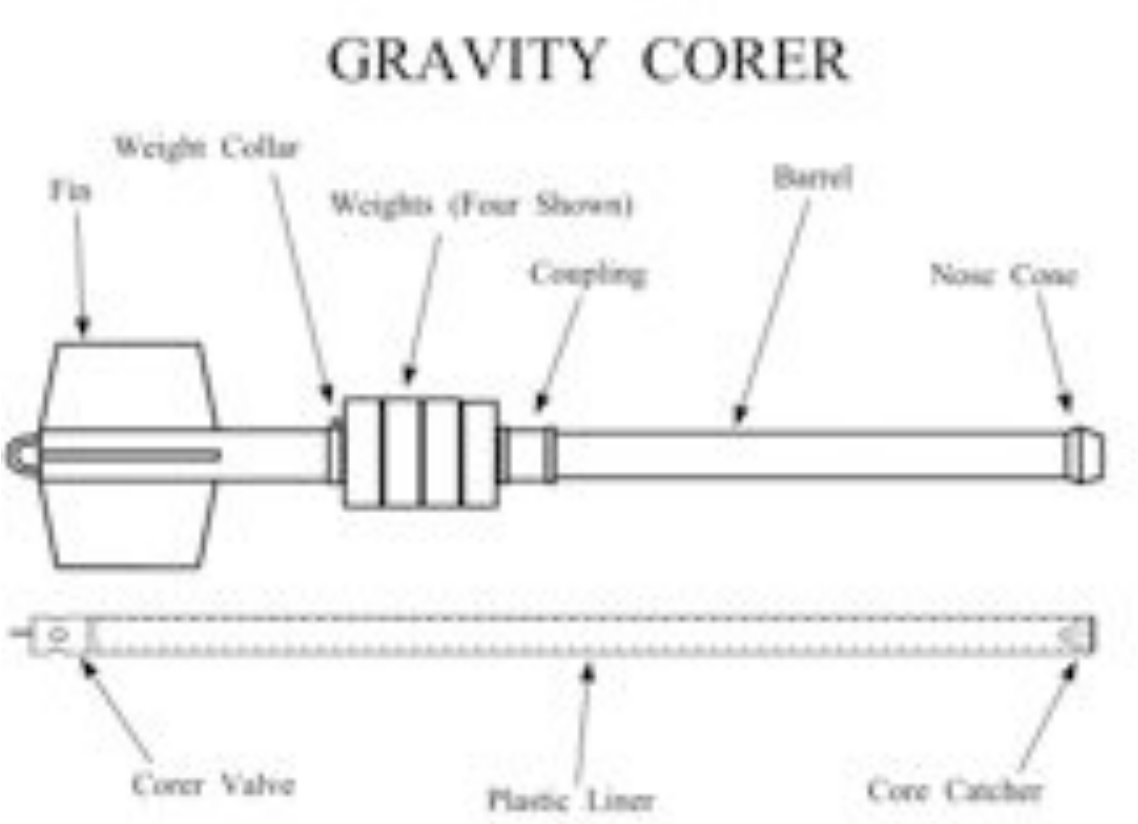

Figure 4. Schematic of a gravity corer, with weights, barrel, nose cone, and core catcher.

Figure 5. The gravity core collection process, clockwise from top left. (1) The corer is dropped into the water, (2) the corer is lowered to depth, (3) after impact, the corer is raised, (4) the corer is hoisted out of the water, (5) the core liner is removed from the barrel, and (6) the core is sealed.

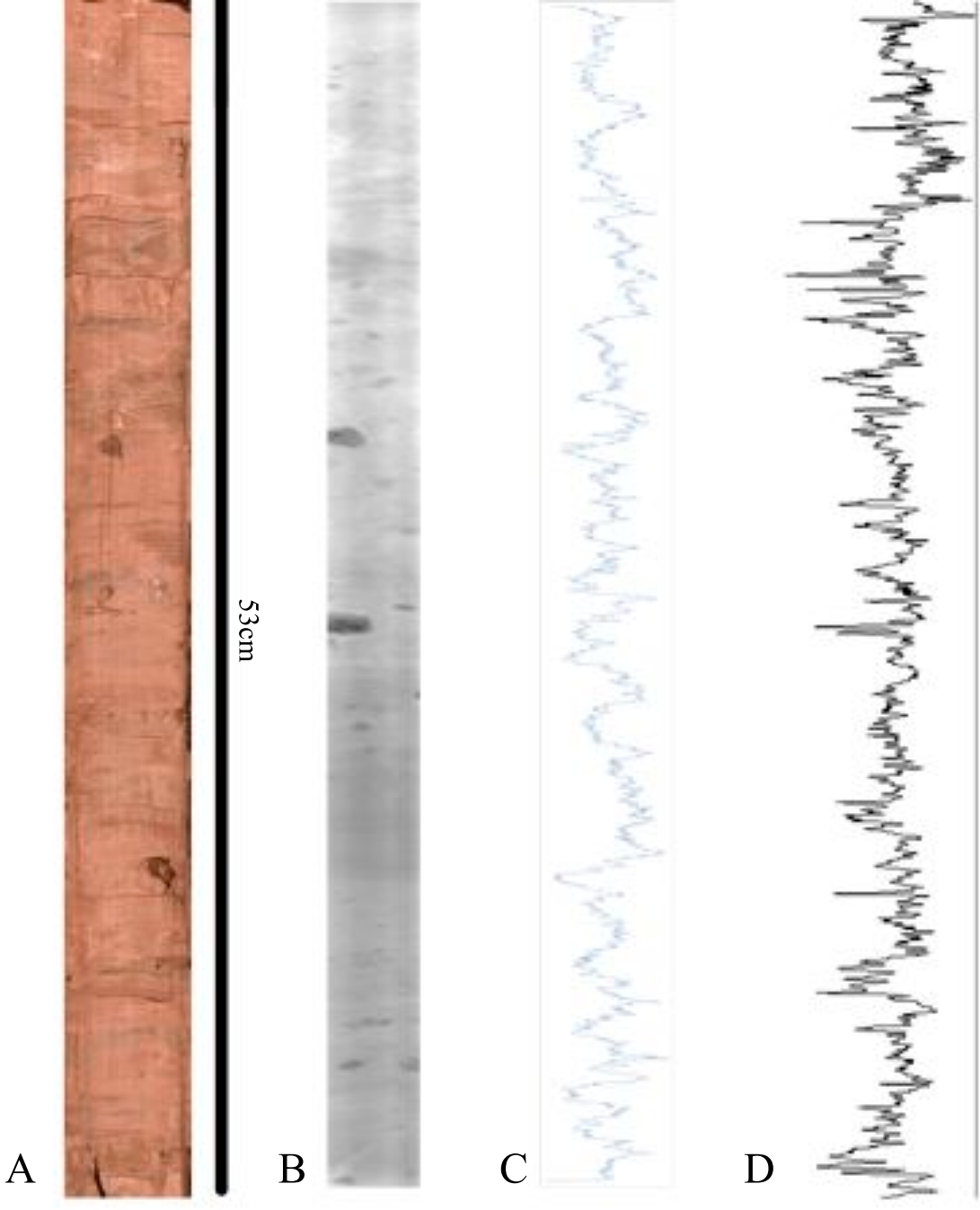

Figure 7. Optical image (A), x-radiograph (B), Ca-Fe ratio profile (C) and sediment color variation profile constructed with ImageJ (D) of GC-12.

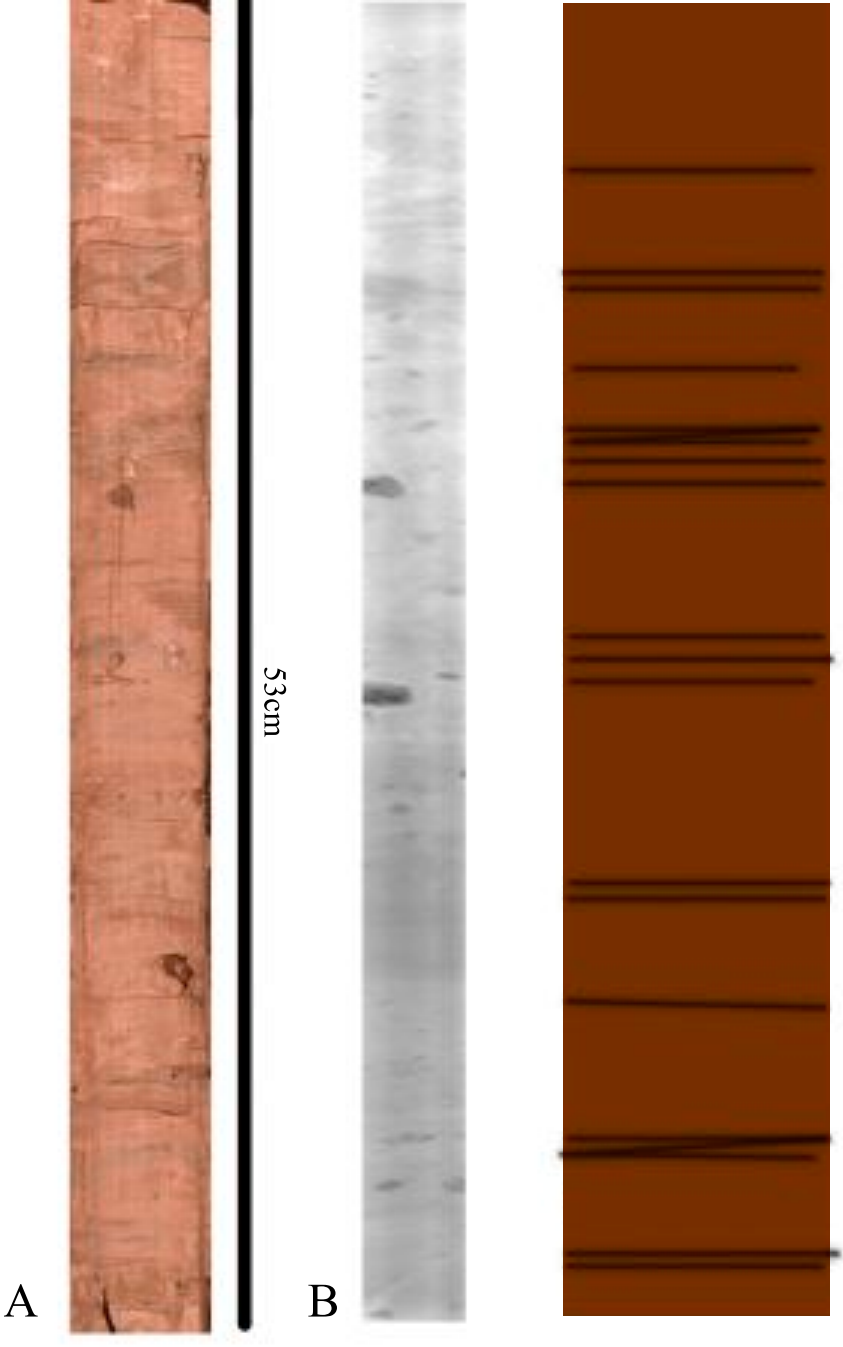

Figure 6. Facies classification of GC-12 alongside optical image (A) and radiograph (B). Brown indicates F1, and black indicates F3.

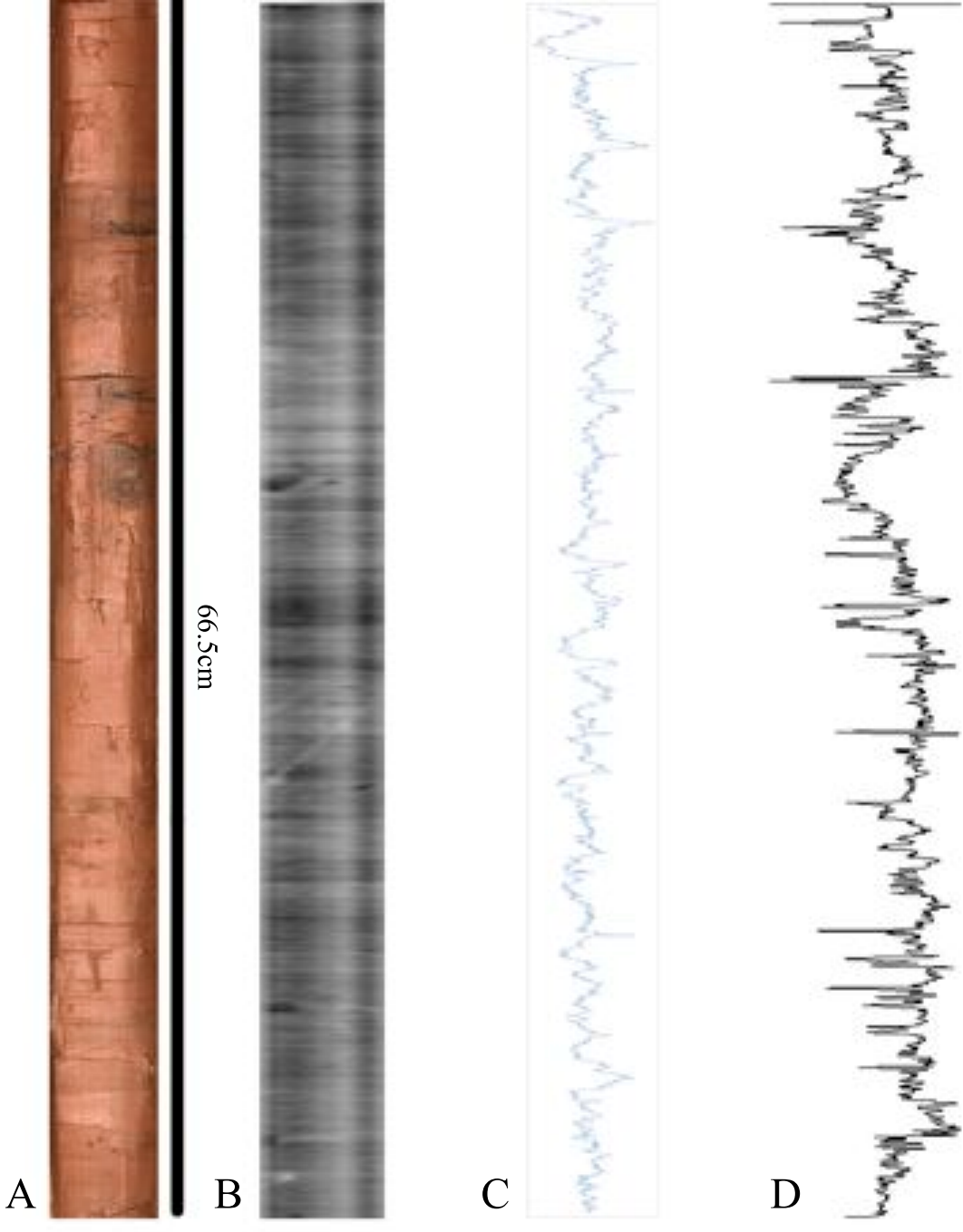

Figure 9. Optical image (A), x-radiograph (B), Ca-Fe ratio profile (C) and sediment color variation profile constructed with ImageJ (D) of GC-24.

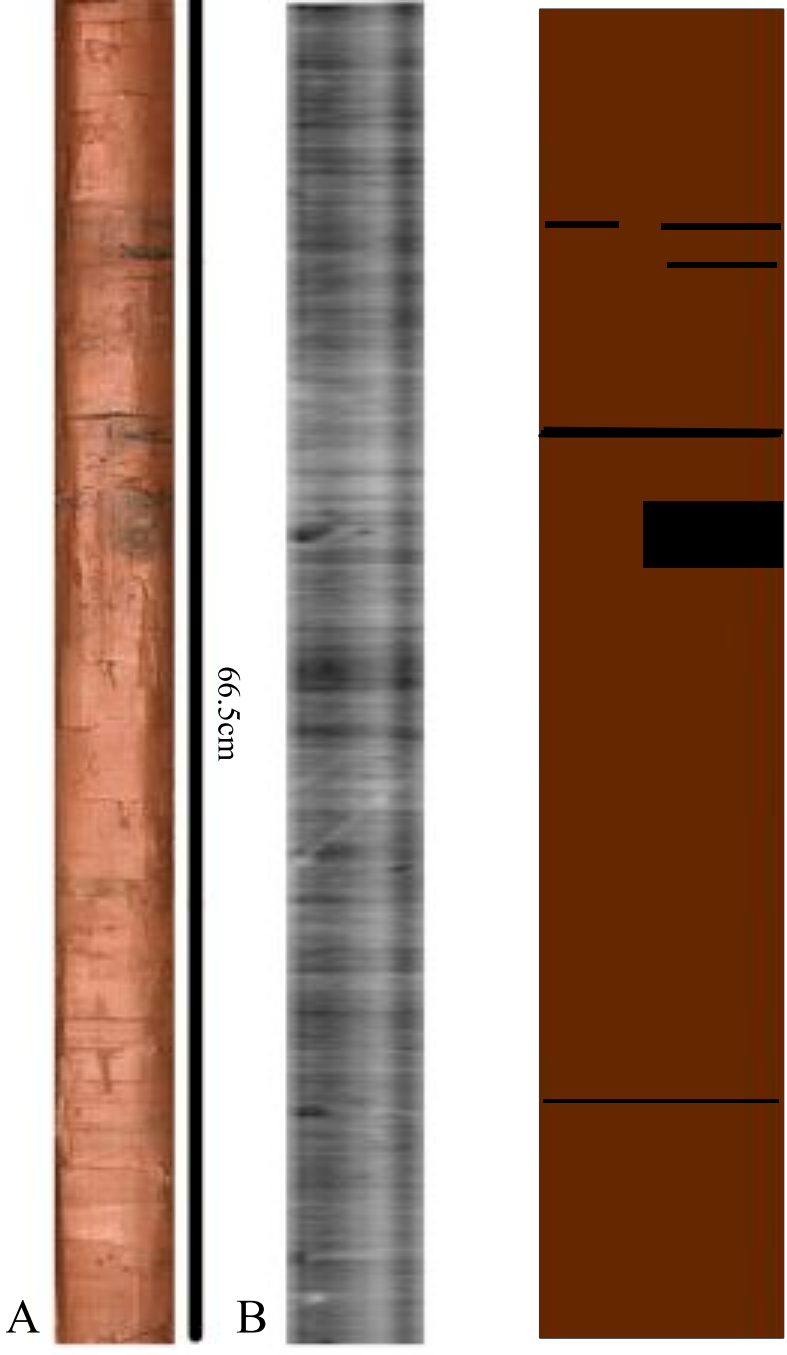

Figure 8. Facies classification of GC-24 alongside optical image (A) and x-radiograph (B). Brown indicates F1, and black indicates F3.

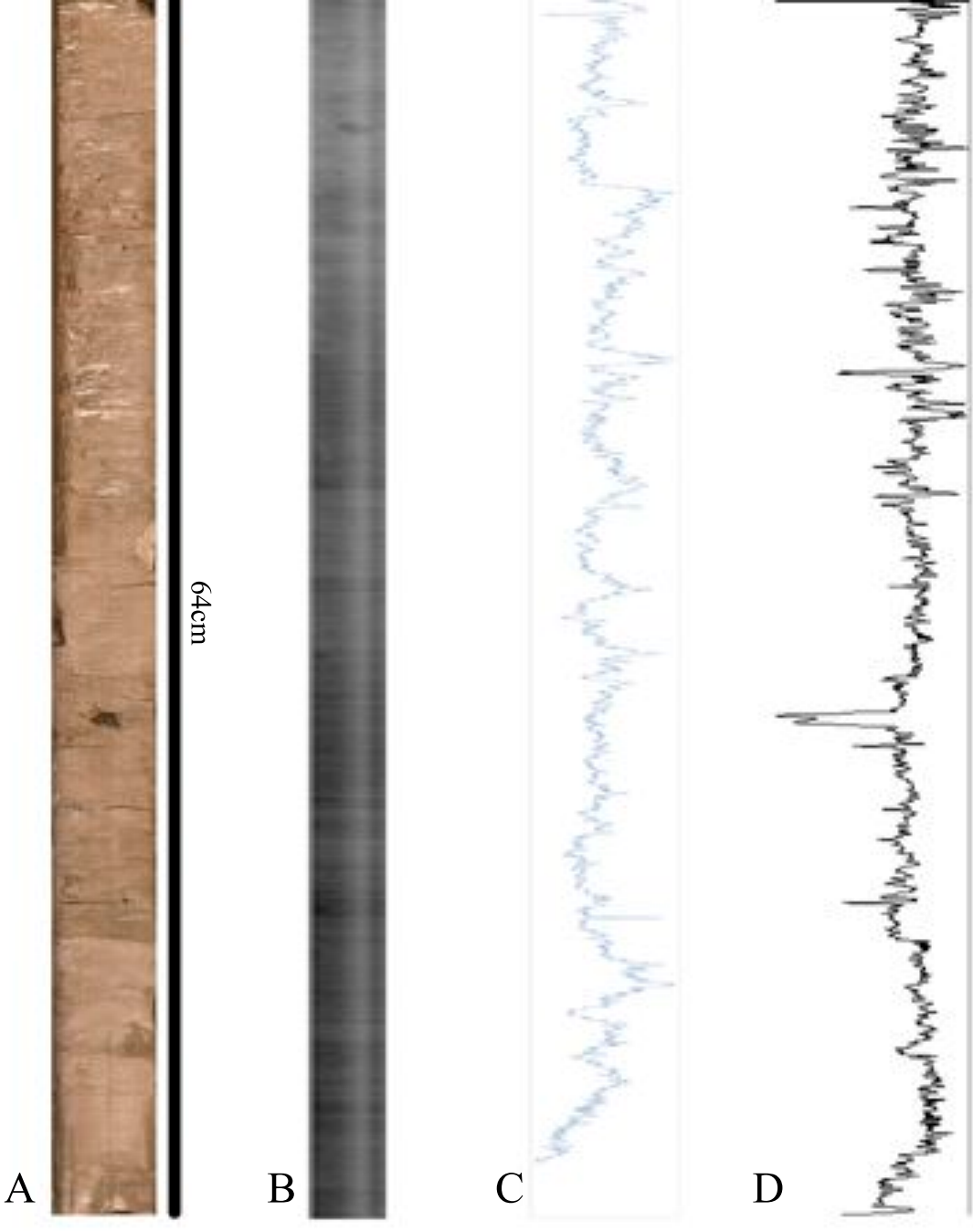

Figure 11. Optical image (A), x-radiograph (B), Ca-Fe ratio profile (C) and sediment color variation profile constructed with ImageJ (D) of GC-25.

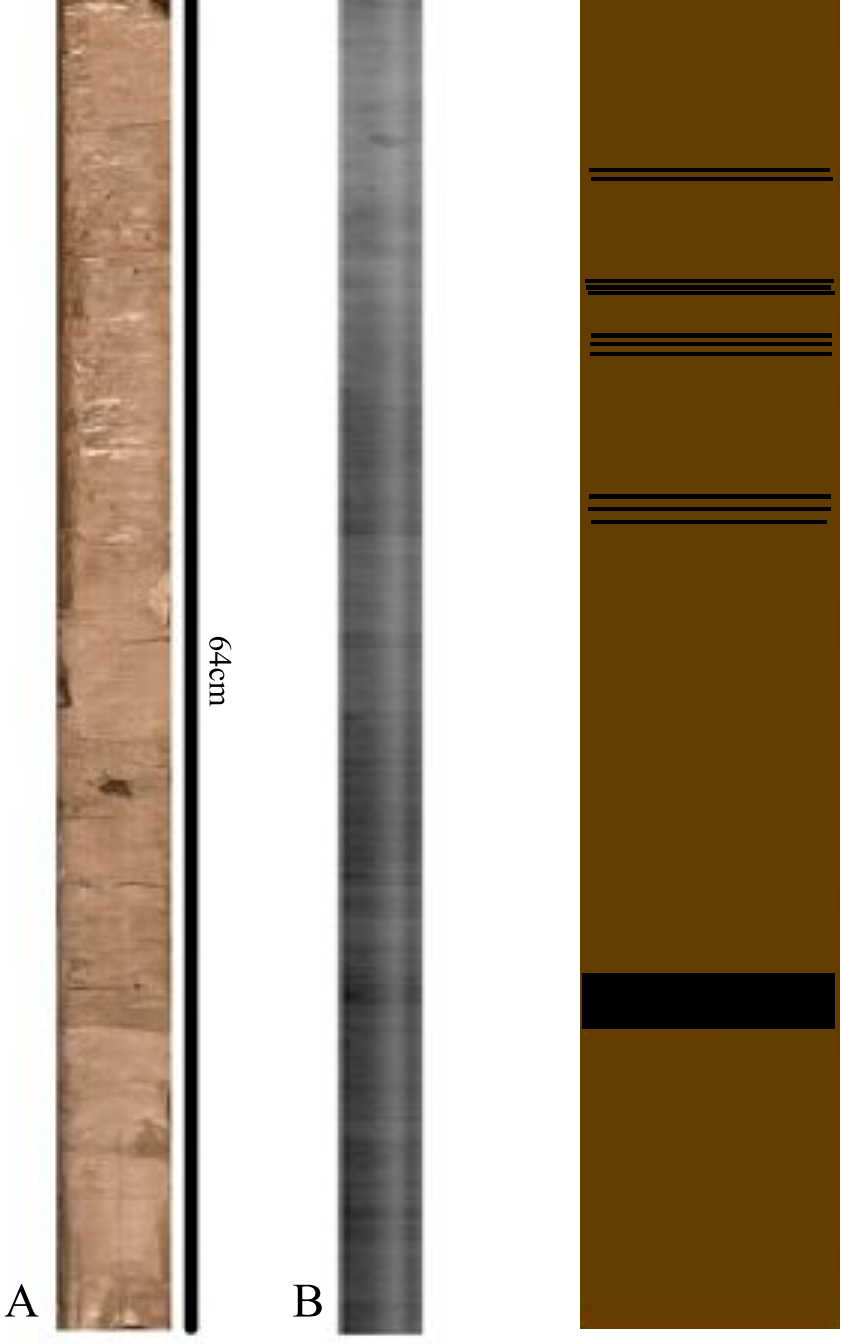

Figure 10. Facies classification of GC-25 alongside optical image (A) and x-radiograph (B). Brown indicates F1, and black indicates F3.

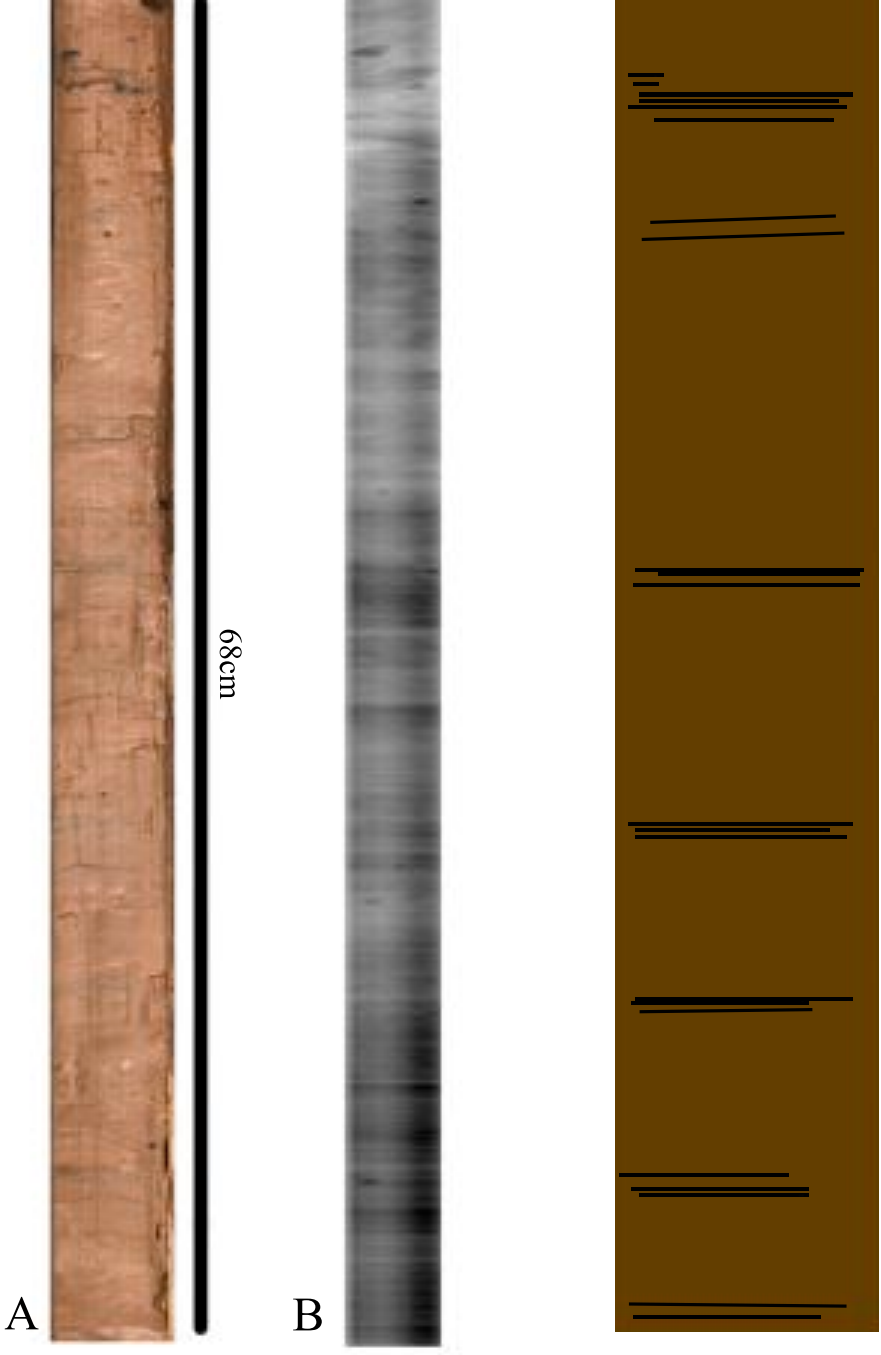

Figure 12. Facies classification of GC-26 alongside optical image (A) and x-radiograph (B). Brown indicates F1, and black indicates F3.

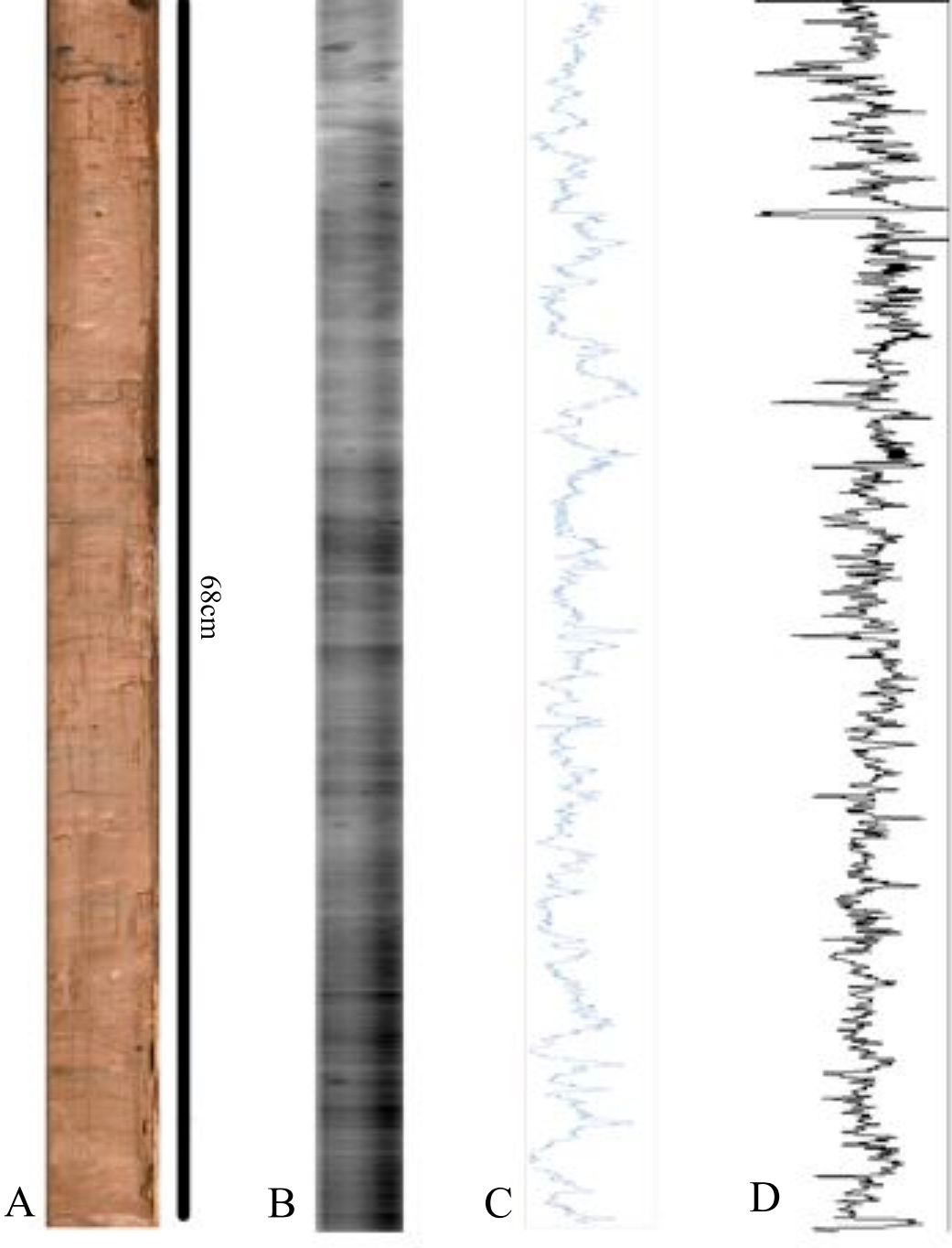

Figure 13. Optical image (A), x-radiograph (B), Ca-Fe ratio profile (C) and sediment color variation profile constructed with ImageJ (D) of GC-26.

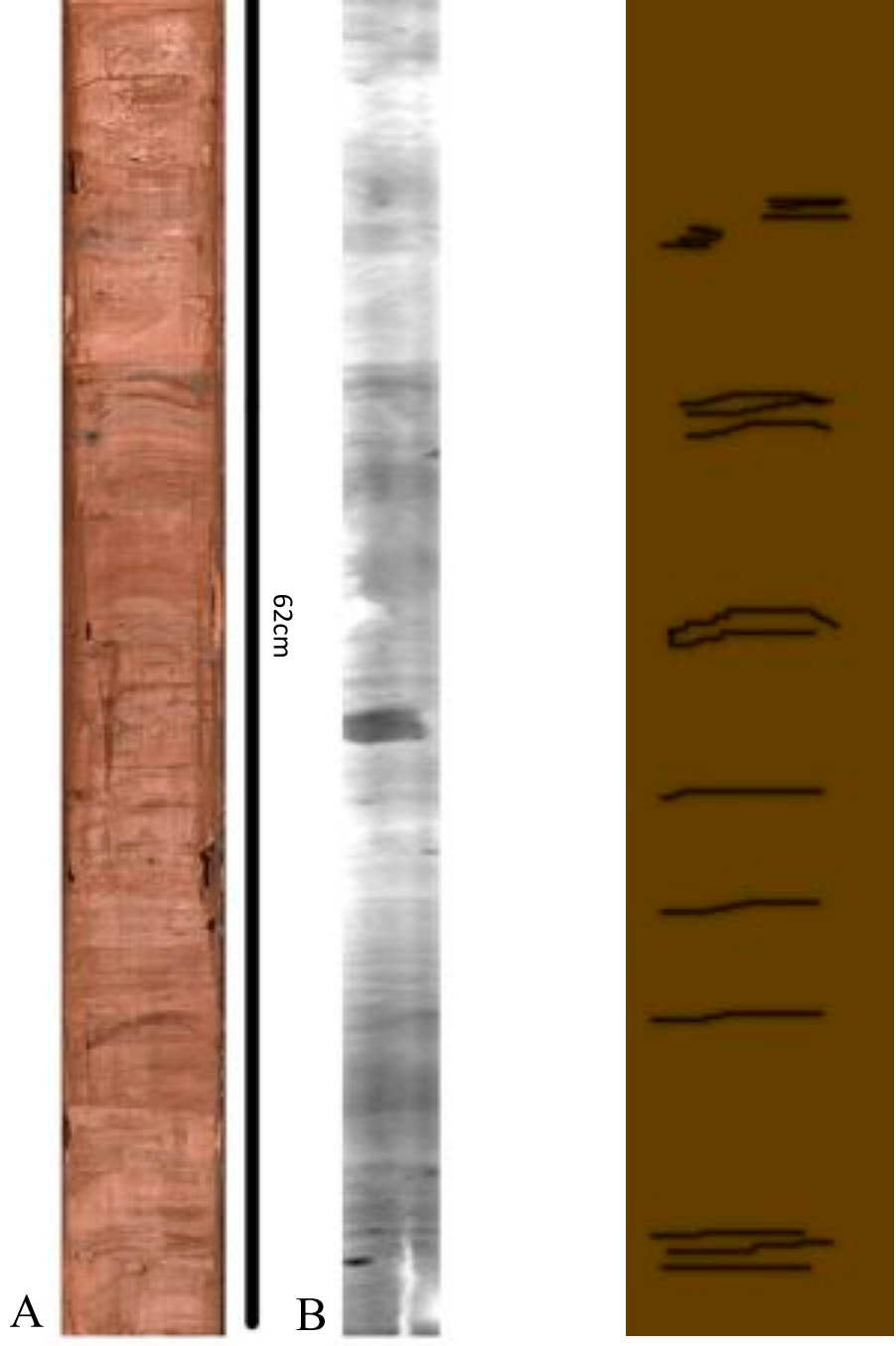

Figure 14. Facies classification of GC-27 alongside optical image (A) and x-radiograph (B). Brown indicates F1, and black indicates F3.

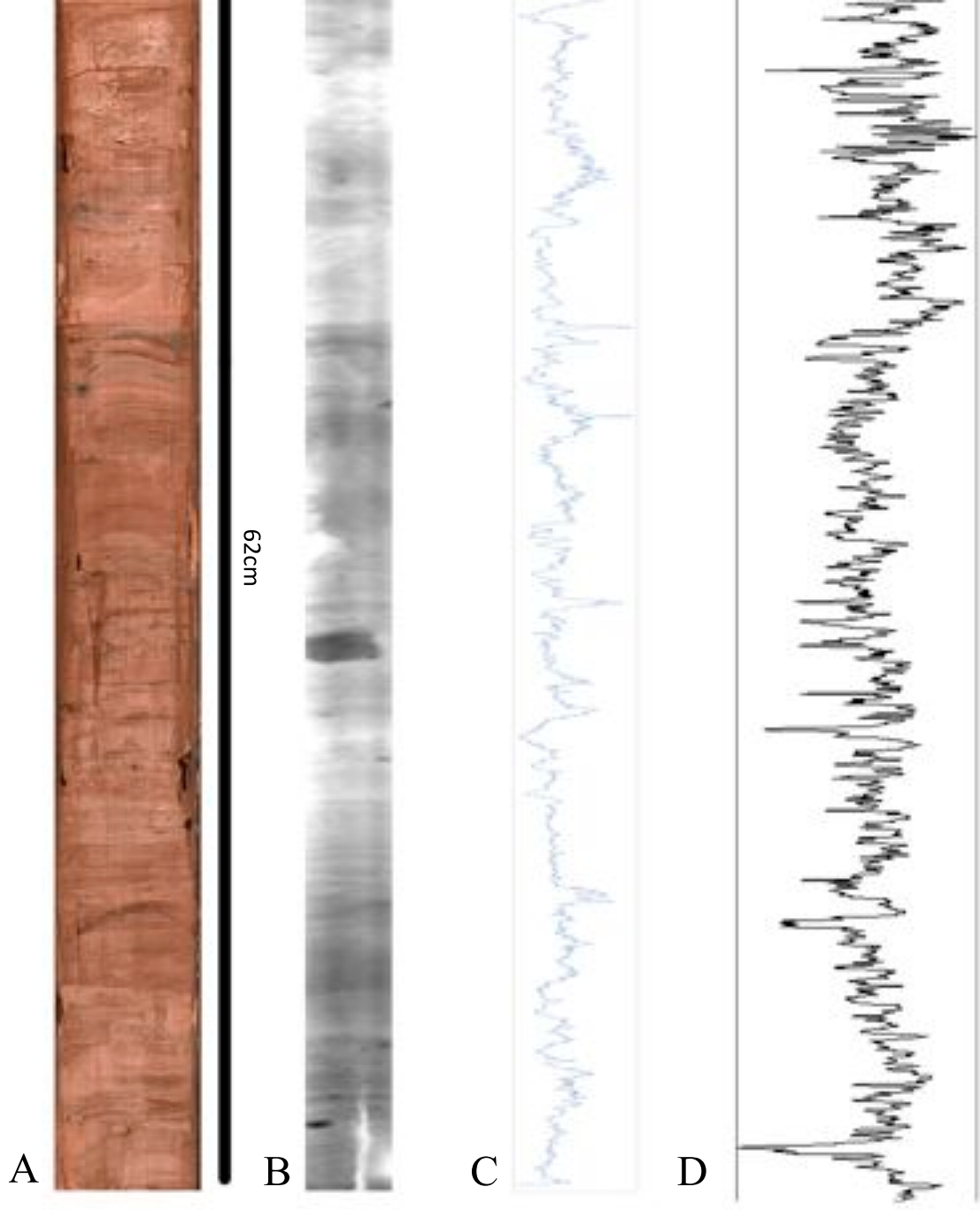

Figure 15. Optical image (A), x-radiograph (B), Ca-Fe ratio profile (C) and sediment color variation profile constructed with ImageJ (D) of GC-27.

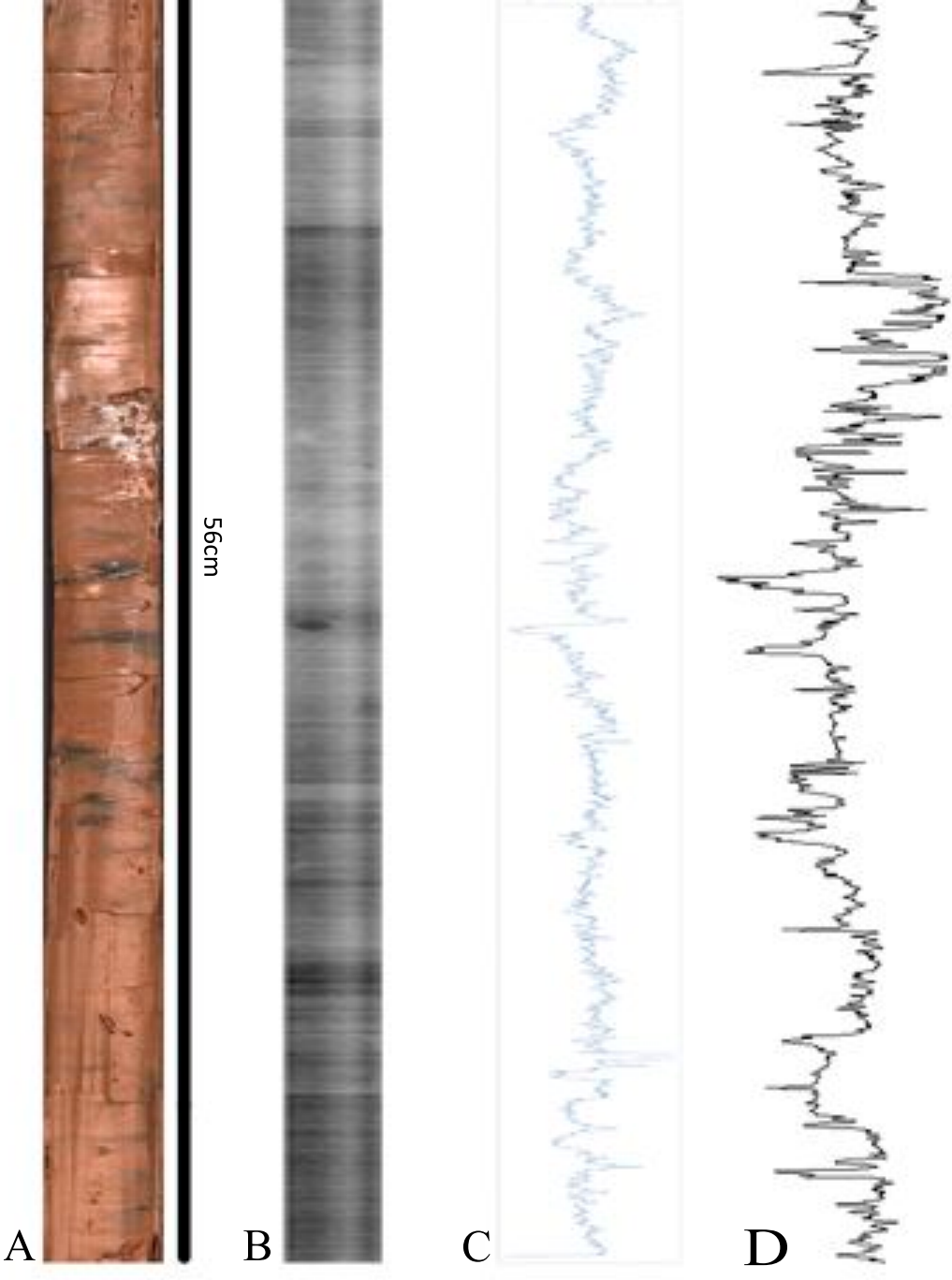

Figure 17. Optical image (A), x-radiograph (B), Ca-Fe ratio profile (C) and sediment color variation profile constructed with ImageJ (D) of GC-29.

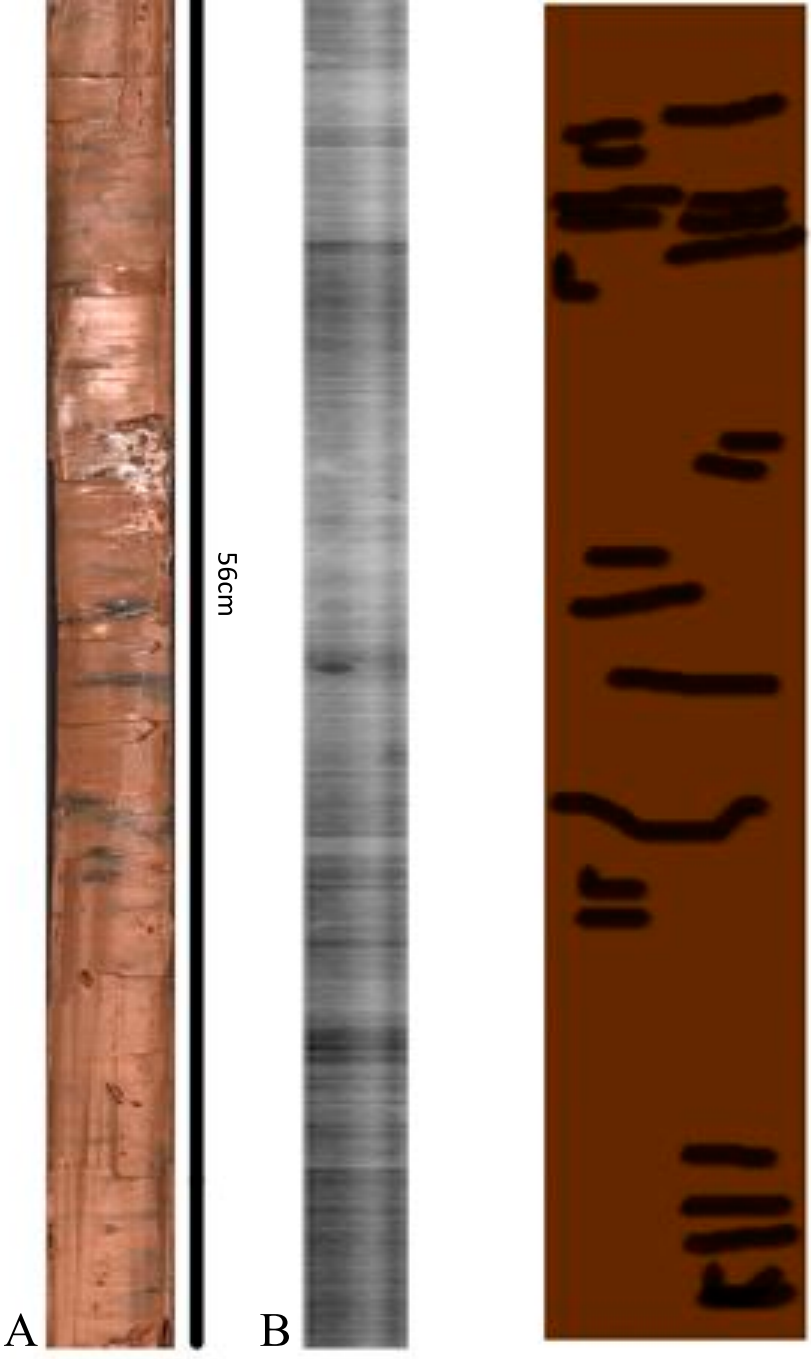

Figure 16. Facies classification of GC-29 alongside optical image (A) and x-radiograph (B). Brown indicates F1, and black indicates F3.

REFERENCES

Alley, R.B., Anandakrishnan, S., Dupont, T.K., Parizek, B.R., and Pollar, D., 2007, Effect of sedimentation on ice-sheet grounding-line stability: Science, v. 315, p. 1838-1841.

Bennett M.R., Hambrey M.J., Huddart D., Glasser N.F. and Crawford K., 1999, The landform and sediment assemblage produced by a tidewater glacier surge in Kongsfjorden, Svalbard: Quaternary Science Reviews, v. 18, p. 1213 – 1246.

Blaszczyk, M., Jania, J.A., Hagen, J.O, 2009, Tidewater glaciers of Svalbard: Recent changes and estimates of calving fluxes: Polish Polar Research, v. 30, no. 2, p. 85-142.

Boulton, G.S., 1990, Sedimentary and sea level changes during glacial cycles and their control on glacimarine facies architecture, eds., Glacimarine Environments: Processes and Sediment, Geological Society Special Publications No. 53, p. 15 – 52.

Cowan, E.A., and Powell, R.D., 1990, Suspended sediment transport and deposition of cyclically interlaminated sediment in a temperate glacial fjord, Alaska, U.S.A., in Dowdeswell, J.A., and Scourse, J.D., eds., Glacimarine Environments: Processes and Sediments, Geological Society Special Publications No. 53, p. 75–90.

Cowan, E.A., and Powell, R.D., 1991, Ice-proximal sediment accumulation rates in a temperate glacial fjord, southeastern Alaska, in Anderson, J.B., and Ashley, G.M., eds., Glacial marine sedimentation; paleoclimatic significance: Geological Society of America Special Paper 261, p. 61–74.

Cowan, E.A., J. Cai, R.D. Powell, K.C. Sermur, V.L. Spurgeon, 1998, Modern tidal rhythmites deposited in a deep-water estuary: Geo-Marine Letters, v. 18, p. 40 – 48.

Cowan, E.A., and Powell, R.D., 2007. High frequency climate signals in fjord sediments of Glacier Bay National Park, Alaska, in Piatt, J.F., and Gende, S.M., eds., Proceedings of the Fourth Glacier Bay Science Symposium, October 26—28, 2004: USGS Scientific Investigations Report 2007-5047, p. 46-49.

Cottier, F., Tverberg, V., Inall, M., Svendsen, H., Nilsen, F., & Griffiths, C, 2005, Water mass modification in an Arctic fjord through cross-shelf exchange: The seasonal hydrography of Kongsfjorden, Svalbard, Journal of Geophysical Research, v.110.

Croudace, I.W., Rindby, A., and Rothwell, R.G., 2006, ITRAX: description and evaluation of a new multi-function X-ray core scanner: in Rothwell, R.G., (Ed.), New Techniques in Sediment Core Analysis: Geological Society, London, Special Publications, v. 267, p. 51-63.

Dallman, W.K., (Ed.), 1999, Lithostratigraphic Lexicon of Svalbard: Tromso, Norsk Polarinstitutt.

Dickin, A.P., 2005, Radiogenic isotope geology, second edition: Cambridge University Press, 492 pp.

Fischer, M.P. and Powell, R.D., 1998, A simple model for the influence of push-morainal banks on the calving and stability of glacial tidewater termini: Journal of Glaciology, 44, 31-41.

Forman, S.L., 1990, Post-glacial relative seal-level history of northwestern Spitsbergen, Svalbard, 1990: Geological Society of America Bulletin, 102, p. 1580 – 1590.

Hjelle, A., 1993: The Geology of Svalbard: Oslo, Norsk Polarinstitutt, 163 pp.

Hop, H., Pearson, T., Hegseth, E.N., Kovacs, K.M., Wiencke, C., Kwansiewski, S., Eiaine, K., Mehlum, F., Gulliksen, B., Wlodarska-Kowlaczuk, M., Lydersen, C., Weslawski, J.M., Cochrane, S., Gabrielsen, G.W., Leakey, R.J.G., Lonne, O.J., Zajaczkowski, M., Falk- Petersen, S., Kendall, M., Wangberg, S.,-A., Bischof, K., Voronkov, A., Y., Kovaltchouk, N.A., Wiktor, J., Poltermann, M., Di Prisco, G., 2002, The marine ecosystem of Kongsfjorden, Svalbard: Polar Research, v. 21, p. 167-208.

Ingolfsson, O., 2008: http://notendur.hi.is/oi/svalbard_geology.htm (accessed 16 October 2011)

Kwok, R, 2009, Outflow of Arctic Ocean Sea Ice into the Greenland and Barents Seas: 1979-2007: Journal of Climate, v. 22, p. 2438 – 2457.

MacLachlan S.E., Cottier F.R., Austin W.E.N., and Howe J.A., 2007, The salinity: d18O water relationship in Kongsfjorden, western Spitsbergen: Polar Research, v. 26, p. 160 – 167.

Melvold, K., and Hagen, J.O., 1998, Evolution of a surge-type glacier in its quiescent phase; Kongsvegen, Spitsbergen, 1964-95. Journal of Glaciology: v. 44, p. 394 – 404.

Norwegian Polar Institute, 2008: http://cruise-handbook.npolar.no/en/kongsfjorden/ (accessed 28 September 2011)

Ó Cofaigh, C., and J.A. Dowdeswell, 2001, Laminated sediments in glacimarine environments: diagnostic criteria for their interpretation, Quaternary Science Reviews: v. 20, p. 1411 – 1436.

O'Neel, 2000, Motion and Calving at Leconite Glacier, Alaska, Master's Thesis, University of Alaska Fairbanks.

Overpeck, J., Hughen, K., Hardy, D., Bradley, R., Case, R., Douglas, M., Finney, K., Gajewski, K., Jacoby, G., Jennings, A., Lamoureux, S., Lasca, A., MacDonald, G., Moore, J., Retelle, M., Smith, S., Wolfe, A., Zielinski, G., 1997, Arctic environmental change of the last four centuries: Science, v. 278, p. 1251 – 1256.

Ottesen, D., Dowdeswell, J.A., Rise, L., 2005, Submarine landforms and the reconstruction of fast-flowing ice streams within a large Quaternary ice sheet: The 2500-km-long Norwegian-Svalbard margin (57°N - 80°N): Geological Society of America Bulletin, v. 117, p. 1033 – 1050.

Poppick, L.N., 2010, Modern depositional processes proximal to a polythermal tidewater glacier complex, Kronebreen-Kongsvegen, Kongsfjorden: Svalbard, Norway (undergraduate thesis): Lewiston, Bates College, 81 p.

Powell, R.D., 1990, Glacimarine processes at grounding-line fans and their growth the ice-contact deltas, in Dowdeswell, J.A., and Scourse, J.D., eds., Glacimarine Environments: Processes and Sediments: Geological Society Special Publications, no. 53, p. 53 – 73.

Powell, R.D., 1991, Grounding-line systems as second-order controls on fluctuations of tidewater termini of temperate glaciers, in Anderson, J.B., and Ashley G.M., eds., Glacial marine sedimentation; Paleoclimatic significance: Boulder, Colorado, Geological Society of America Special Paper 261.

Powell, R.D., and E.W. Domack, 1995, Modern glaciomarine environments, In: Menzies, J. (Ed.), Glacial Environments, Vol. 1: Modern Glacial Environments: Processes, Dynamics and Sediments. Butterworth-Heinemann, Oxford, p. 445 - 486.

Powell R.D., 2003, Subaquatic Landsystems: Fjords in Evans D.J.A.. ed., Glacial Landsystems, ch. 13, p. 313 – 347.

Rothwell, R.G., Hoogakker, B., Thomson, J., Croudace, I.W., & Frenz, M, 2006, Turbidite emplacement on the southern Balearic Abyssal Plain (western Mediterranean Sea) during Marine Isotope Stages 1-3: an application of ITRAX XRF scanning of sediment cores to lithostratigraphic analysiin Rothwell, R.G., (Ed.), New Techniques in Sediment Core Analysis: Geological Society, London, Special Publications, v. 267, p. 51-63.

Samadhisoft.com, 2008: http://samadhisoft.com/2008/01/18/obscure-information-anyone-the-treaty-of-svalbard/ (accessed 27 September 2011).

Smith, J. and M.D. Melville, 2004, Iron monosulfide formation and oxidation in darin-bottom sediments of an acid sulfate soil environment: Applied Geochemistry, v. 19, p. 1837 – 1835.

Stewart, T.G., 1991, Glacial marine sedimentation from tidewater glaciers in the Canadian High Arctic, in Anderson, J.B., and Ashley G.M., eds., Glacial marine sedimentation; Paleoclimatic significance: Boulder, Colorado, Geological Society of America Special Paper 261. p. 95 – 105.

Svalbard REU Program, 2004: http://www.mtholyoke.edu/proj/svalbard/project.shtml (accessed 27 September 2011).

Svendsen, H., Beszczynska-Møller, A., Hagen, J. O., Lefauconnier, B., Tverberg, V., Gerland, S., Ørbaek, J. B., Bischof, K., Papucci, C., Zajaczkowski, M., Roberto, A., Bruland, O., Wiencke, C., Winther, J.-G. & Dallmann, W. 2002. The physical environment of Kongsfjorden-Krossfjorden, an Arctic fjord system in Svalbard: Polar Research, v. 21, p. 133-166.

Trusel, Luke D., Cumpston R.M., Powell R.D., Brigham-Grette, J. 2010. Modern glacimarine processes and potential future behaviour of Kronebreen and Kongsvegen tidewater glaciers, Kongsfjorden, Svalbard. Geological Society, London, Special Publications 2010; v. 344, p. 89-102.

Visbeck M.H., Hurrell J.W., Polvani L., Cullen H.M., 2001, The North Atlantic oscillation: Past, present, and future: Proceedings of the National Academy of Sciences of the United States of America, v. 98., p. 12876 – 12877

Winther J.G, Godtliebsen F., Gerald S., Isachsen P.E., 2002, Surface albedo in Ny-Alesund, Svlabard: variability and trends during 1981 – 1997: Global and Planetary Change, v. 32, p. 127 – 139.

Zaborska A., Pempkowiak J., Papucci C., 2006, Some sediment characteristics and sedimentation rates in an arctic fjord (Kongsfjorden, Svalbard): Annual Environmental Protection, v. 8, p. 79-96.

Zajaczowski, M., Nygard, H., Hegseth, E.N., and Berg, J., 2010, Vertical flux of particulate matter in an Arctic fjord: the case of lack of the sea-ice cover in Adventfjorden 2006 – 2007: Polar Biology, v. 33, no. 2, p. 223 – 239.

Zajaczowski, M., M. Wlodarska-Kowalczuk, 2007, Dynamic sedimentary environments of an Arctic glacier-fed river estuary (Advenfjorden, Svalbard). I Flux, deposition, and sediment dynamics: Estuarine, Coastal and Shelf Science, v. 74, p. 285 – 296.